

Fast Uncertainty Quantification for Active graph-SLAM

Julio A. Placed, *Student Member, IEEE*, and José A. Castellanos, *Senior Member, IEEE*

Abstract—Quantifying uncertainty is a key stage in autonomous robotic exploration, as it allows identifying the most informative actions to execute. However, dealing with full Fisher Information Matrices (FIM) is computationally heavy and may become intractable for online systems. In this work, we study the paradigm of active graph-SLAM formulated over $SE(n)$, and propose a general relationship between the full FIM and the Laplacian matrix of the underlying pose-graph. Therefore, the optimal set of actions can be estimated by maximizing optimality criteria of the weighted Laplacian instead of that of the FIM. Experimental validation shows that our method leads to equivalent results in a fraction of the time. Based on this, we present an online active graph-SLAM system capable of rapidly selecting D-optimal actions and that also outperforms other state-of-the-art methods.

Index Terms—Active SLAM, optimality criteria, autonomous agents, robotic exploration, topology, connectivity.

I. INTRODUCTION

AUTONOMOUS robotic exploration refers to the paradigm of controlling a robot in order to acquire an accurate representation of the environment (i.e. map) in a finite time horizon. Simultaneous Localization and Mapping (SLAM) deals with the base problem of incrementally building a map of the environment while at the same time locating the robot on it. Many approaches have been developed to solve this problem, although the interest of this paper relies on pose graph-SLAM methods (also known as Pose SLAM), that can be intuitively formulated using a graph representation where nodes encode the robot poses, and edges encode the constraints between them. This SLAM variant is built on the idea that the map representation (e.g. an occupancy grid as in this paper) can be retrieved once the robot states have been properly estimated [1], [2]. After solving the data association problem and building the graph, it all comes down to finding the optimal nodal configuration via Maximum Likelihood (ML), that is, finding the set of robot poses that minimizes the negative log-likelihood cost function of the observations. See [3], [4], [2], [5] and references there in.

Active SLAM expands the previous problem so as to include the optimal choice of actions the robot should execute to get the best possible representation of the environment. This new problem, erected on the basis of *active localization* [6], can be formally defined as the paradigm of controlling a robot which is performing SLAM so as to reduce the uncertainty of its localization and the map's representation [7], [8]. This

involves reasoning over the probabilistic states (beliefs) under uncertainty, a problem also referred to as Belief Space Planning (BSP) [9], [10].

Active SLAM is generally divided in three phases [11]:

- i) the identification of all possible locations to explore,
- ii) the evaluation of the utility associated to the actions that would take the robot from its current position to each of those locations, and
- iii) the selection and execution of the optimal set of actions.

In the first stage, ideally, all possible actions to reach all possible locations should be evaluated, although easily proves to be intractable due to the dimensionality of the map space, and also of the action set in some applications. In practice, the most common approach is the identification of the points which lie between the known and unknown regions of the map: frontiers.

During the second step, the utility of each set of actions is traditionally computed by quantifying the uncertainty in the estimation of the two target random variables: the robot's pose and the map's representation. So far, this matrix quantification has been based either on Theory of Optimal Experimental Design (TOED) or Information Theory (IT), and is just a scalar mapping of the covariance matrix [12]. In any case, these utility functions must find the equilibrium between exploring new areas and exploiting those previously seen (*exploration-exploitation dilemma*). The most common method is to analyze the FIM iteratively to compute the expected information gain after the execution of a set of actions via Shannon's entropy [13], [14], [15], [16]; although some recent works rely, preferably, on D -optimality criterion that stems from TOED [17]. Both map and pose uncertainties are sometimes treated as independent [18] and sometimes combined linearly [11], although in this case parameter tuning is needed due to the discrepancy in the values of both terms. Carrillo *et al.* [19] avoid this manual tuning by correcting map Shannon's entropy with Rényi's entropy, which encodes a metric of the robot's uncertainty (D -optimality).

Third phase consists in executing the set of actions with highest utility. Ideally, the full sequence would be repeated until the whole environment is explored, although in practice it is carried out until certain *stopping criteria* are met, which usually rely on time or coverage constraints (e.g., during 10 minutes or until 95% of the environment is mapped) for easiness. The continuous acquisition of redundant information could even result in map inconsistencies due to wrong loop closures. However, note that the previous constraints are not valid when exploring truly unknown environments. In this respect, the evolution of certain optimality criteria from TOED has been identified as promising to know when to stop

This work was supported by the MINECO project PID2019-108398GB-I00 and DGA Group T45-20R.

The authors are with the Instituto de Investigación en Ingeniería de Aragón (I3A), Universidad de Zaragoza, C/María de Luna 1, 50018, Zaragoza, Spain e-mail: {jplaced,jacaste}@unizar.es.

exploration [5], although no further research has been done in the topic.

In any case, the use (i.e. propagation, store and analysis) of dense covariance matrices quickly becomes intractable in online active SLAM. For example, approaches that require computing the determinant of the *a posteriori* covariance matrix, are $\mathcal{O}(n^3)$ complex in general, with n the dimension of the full state. In order to lessen the computational load, most works resort to sparse information matrices [20] or use sparsified representations, as in [19] and [21]. In this vein, Khosoussi *et al.* [22] recently observed that classical optimality criteria in active graph-SLAM are closely related to the connectivity of the underlying pose-graph. In particular, they show the existing relationship between the number of spanning trees of a graph and the covariance determinant (traditional *D*-optimality), and that between the algebraic connectivity and the covariance minimum eigenvalue (*E*-optimality); for 2D graph-SLAM and assuming the covariance matrix block-isotropic and constant through measurements.

The idea of the topology of a graph being related to its optimality, however, was already proposed four decades ago, when Cheng [23] realized that a graph with the maximum number of spanning trees is *D*-optimal, and thus related two problems (from Graph Theory and TOED) that had always been viewed differently. Work of Khosoussi *et al.* was extended in [24] to account for variable uncertainty in compass- and 2D-SLAM, under the assumption of uncorrelated robot's covariance; and later in [25], where they also relate the graph's node degree with the FIM's trace (traditional *T*-optimality), for the particular case of Pose SLAM in which orientation is defined with rotation matrices. Exploitation of the graph structure was also recently transferred to the domain of information-theoretic BSP. Kitanov and Indelman [26] prove that a metric based on the number of spanning trees is also a good approximation of the estimated posterior entropy; a reasonable fact since it ultimately depends on the covariance determinant just like *D*-optimality does. They also present a faster approximation based on the relationship between the graph's node degree and Von Neumann entropy, although it fails to select the optimal actions in some cases (just as *T*-optimality would). The graphical approaches show a reduction in time complexity of an order of magnitude.

Following all these ideas, instead of maximizing optimality criteria of the FIM, the optimal set of actions in active SLAM could be found through the maximization of graph connectivity indices. Chen *et al.* [17] build a 2D active SLAM algorithm that achieves uncertainty minimization by leveraging the graphical structure of the underlying pose-graph.

A. Contributions

The main contributions of this work are the following:

- 1) On the basis of Graph Theory, differential models and [22], we derive a general theoretical relationship between the FIM of a graph-SLAM problem formulated over the Lie group $SE(n)$, and the Laplacian matrix of the underlying pose-graph. On top of that, we establish a strong link between the spectrum of both matrices and

relate the FIM's optimality criteria to the graph connectivity indices. Contrarily to [24], [25], covariance of the measurements is not necessarily block-isotropic, formulation is done over $SE(n)$ allowing its natural application to 3D, and modern optimality criteria are used. Note that these elements are key for active SLAM applications, since (i) only differential representations maintain the monotonicity of the decision making criteria [27], and (ii) the use of traditional criteria is not suitable for active SLAM. For example, traditional *D*-optimality can rapidly tend to zero and since the size of the FIM grows over time, comparison of determinants of matrices with different sizes is unfair [28].

- 2) We validate the proposed relationships and analyze time complexity in several 2D and 3D datasets, showing that using the structure of the underlying pose-graph results in equivalent results for the task of active SLAM, if the pose-graph is properly weighted. On average, this method requires just 10% of the time traditional computations would and results in estimation errors of 2%; but, more importantly, it always maintains the same trend.
- 3) Finally, we present an online *D*-optimal active SLAM system based on the proposed relationships and their low computational load. In contrast to [19], fast evaluation of utility is possible since both the robot and map's uncertainties are embedded in the (predicted) graphs. We benchmark our system with five other methods representing both traditional approaches and the state-of-the-art. Our method outperforms them all on many metrics, demonstrating its usefulness for autonomous exploration applications. It has been developed for ROS Noetic and Gazebo and has been released [here](#)¹.

Please note that this work is an extension of our previous conference paper [29]. Here, we present a complete and clear derivation of the theoretical results, supplemented in appendices, and propose an approximation relationship between optimality criteria of the FIM and the Laplacian for the general case of variable uncertainty. We thoroughly extend the validation experiments. In addition, we have significantly improved and analyzed our online active SLAM system, which is now publicly available.

B. Paper Structure

The rest of the paper is organized as follows. Section II presents preliminary contents about graph-SLAM, optimality criteria, Graph Theory and its spectrum. Section III contains the theoretical contributions of this paper that relate graph connectivity indices with optimality criteria. The experimental validation is shown in Section IV. Section V contains the online active SLAM approach. Finally, the paper is concluded in Section VI, where future work is also outlined. Appendix A provides a brief introduction to Lie groups, Appendix B contains some properties of the Kronecker product and Appendix C shows the proof of the equivalences between optimality criteria of covariance and information matrices. Additional validation results appear in Appendix D.

¹https://github.com/JulioPlaced/active_graph_slam

II. PRELIMINARIES

A. Graph-based SLAM

Graph-based SLAM approaches employ a graphical representation to solve the SLAM estimation problem. Nodes in the graph represent the poses of the variables of interest (i.e. the robot's location and the map points), while edges represent the sensor measurements. The process of generating constraints between nodes from the observations is known as data association and is usually bounded to the most likely topology in order to restrain complexity. Thus, under the assumption of observations affected by Gaussian noise, an edge will encode the relative pose between two nodes and the associated covariance matrix. Edges may represent a constraint related to a sensor measurement (e.g. odometry) or to the detection of a loop closure. The work in this paper is particularly focused on pose-graphs, which restrict the previous representations by encoding only the robot's poses in vertices. In such cases, rather than using a landmark-based representation, the map is usually built incrementally as an occupancy grid via, e.g. scan matching, and updated after a loop closure. This map representations discretize the environment in known (occupied or free) and unknown cells.

In any case, once the graph is built and the data association problem solved, the goal of the graph-SLAM algorithm is to compute the (Gaussian-approximated) posteriors over the robot poses. That is, to find the nodal configuration that maximizes the likelihood of the observations [2]. The following optimization problem may be solved using, e.g., Gauss-Newton or Levenberg-Marquardt techniques:

$$\begin{aligned} \mathbf{x}^* &= \arg \min_{\mathbf{x}} \mathbf{F}(\mathbf{x}) \\ \text{s.t. } \mathbf{F}(\mathbf{x}) &= \sum_{j=1}^m \mathbf{F}_j(\mathbf{x}) = \sum_{j=1}^m \mathbf{d}_j^T(\mathbf{x}) \Sigma_j^{-1} \mathbf{d}_j(\mathbf{x}) \end{aligned} \quad (1)$$

where \mathbf{x} denotes the variable of interest (i.e. robot poses), \mathbf{F} is the cost function (negative log likelihood) of all observations, m the number of edges of the pose-graph, and \mathbf{d}_j and Σ_j the estimation error and covariance associated to the j -th edge.

B. Optimality Criteria

While performing active SLAM, decision making comes down to computing the utility of executing a certain set of actions or, equivalently, to quantifying the uncertainty that such set of actions would lead to. Kiefer [30], on the basis of TOED, shows that there is indeed a family of mappings that quantify uncertainty, i.e. $\|\Sigma\| \rightarrow \mathbb{R}$, which are dependent of just one parameter (p):

$$\|\Sigma\|_p \triangleq \left(\frac{1}{\ell} \text{trace}(\Sigma^p) \right)^{\frac{1}{p}} \quad (2)$$

where ℓ is the dimension of the state vector to be estimated, $(x_1, \dots, x_\ell)^T$, and $\Sigma \in \mathbb{R}^{\ell \times \ell}$ is the symmetric, positive semi-definite covariance matrix which measures its uncertainty. The preferred set of actions will be that with lowest $\|\Sigma\|_p$. Note

that the same analysis could be done on the information matrix, $\Phi = \Sigma^{-1}$.

This information function may be particularized for the different values of p as follows [12],

$$\|\Sigma\|_p = \begin{cases} \sqrt[p]{\frac{1}{\ell} \text{trace}(\Sigma^p)} & \text{if } 0 < |p| < \infty \\ \det(\Sigma)^{\frac{1}{\ell}} & \text{if } p = 0 \end{cases} \quad (3)$$

and expressed in terms of the eigenvalues of Σ , $(\lambda_1, \dots, \lambda_\ell)$, by leveraging the properties of a matrix power:

$$\|\Sigma\|_p = \begin{cases} \left(\frac{1}{\ell} \sum_{k=1}^{\ell} \lambda_k^p \right)^{\frac{1}{p}} & \text{if } 0 < |p| < \infty \\ \exp \left(\frac{1}{\ell} \sum_{k=1}^{\ell} \log(\lambda_k) \right) & \text{if } p = 0 \end{cases} \quad (4)$$

In essence, utility functions are functionals of the eigenvalues of Σ . Four modern optimality criteria are inferred from equation (4):

- *T-optimality criterion* ($p = 1$): captures the average variance, computed as the normalized trace of the covariance matrix (hence its name). Computation of this metric is fast, although it is possible for a single element to drive the whole metric and thus it may perform similar to just evaluating the highest eigenvalue [8].

$$T\text{-opt} \triangleq \frac{1}{\ell} \sum_{k=1}^{\ell} \lambda_k \quad (5)$$

- *D-optimality criterion* ($p = 0$): captures the volume of the whole variance (hyper) ellipsoid. Its name comes from its classical formulation in which the covariance determinant was used. In addition, this is the only criterion that holds the monotonicity property under both absolute and differential representations of uncertainty [27]. Modern formulation of this criterion is as follows:

$$D\text{-opt} \triangleq \exp \left(\frac{1}{\ell} \sum_{k=1}^{\ell} \log(\lambda_k) \right) \quad (6)$$

- *A-optimality criterion* ($p = -1$): captures the harmonic mean variance. It is sensitive to outliers with values much smaller than the rest of the data, in contrast to *T-opt* which just neglects them; and insensitive to extremely large ones.

$$A\text{-opt} \triangleq \left(\frac{1}{\ell} \sum_{k=1}^{\ell} \lambda_k^{-1} \right)^{-1} \quad (7)$$

- *\tilde{E} -optimality criterion* ($p \rightarrow \pm\infty$): approximates the uncertainty using a single eigenvalue. Despite its computation is fast, this criterion tends to be too optimistic by underestimating the covariance (for the case of the minimum eigenvalue).

$$E\text{-opt} \triangleq \min(\lambda_k : k = 1, \dots, \ell) \quad (8)$$

$$\tilde{E}\text{-opt} \triangleq \max(\lambda_k : k = 1, \dots, \ell) \quad (9)$$

C. Graph Theory

A strict undirected graph is defined by the ordered pair of sets $\mathcal{G} \triangleq (\mathcal{V}, \mathcal{E})$, where $\mathcal{V} = \{\mathbf{v}_0, \dots, \mathbf{v}_n\}$ is the set of vertices and $\mathcal{E} = \{\mathbf{e}_1, \dots, \mathbf{e}_m\} \subset \{\{\mathbf{v}_i, \mathbf{v}_k\} \mid \mathbf{v}_i, \mathbf{v}_k \in \mathcal{V}, \mathbf{v}_i \neq \mathbf{v}_k\}$ the set of edges. Their dimensions will be denoted as $|\mathcal{V}| = n$ and $|\mathcal{E}| = m$. The adjacency matrix of the graph, $\mathbf{A} \in \{0, 1\}^{n \times n}$, is a square matrix which columns and rows represent the nodes of the graph and each element $a_{i,k}$ is equal to one if the nodes v_i and v_k are connected and zero otherwise. Note that the diagonal will be zero. The degree matrix, $\mathbf{D} \in \mathbb{N}^{n \times n}$, is a diagonal matrix in which each element is given by:

$$d_{i,k} \triangleq \begin{cases} \deg(\mathbf{v}_i) & \text{if } i = k \\ 0 & \text{otherwise} \end{cases} \quad (10)$$

where $\deg(\mathbf{v}_i)$ is the degree of the i -th vertex, i.e. the number of other nodes it is connected to. The incidence matrix, \mathbf{Q} , shows the connections between vertices and edges. It can be defined as a concatenation of m column vectors, each of them associated to an edge. That is,

$$\mathbf{Q} = (\mathbf{q}_1, \mathbf{q}_2, \dots, \mathbf{q}_m) \in \{-1, 0, 1\}^{n \times m} \quad (11)$$

The column block associated to the edge \mathbf{e}_j , that connects \mathbf{v}_i and \mathbf{v}_k , will be denoted as \mathbf{q}_j . All elements of this matrix will be zero with the exception of those associated to the vertices incident upon \mathbf{e}_j . That is, the i -th and k -th elements of \mathbf{q}_j , which will be $[q_j]_i = -[q_j]_k = 1$. The Laplacian (or admittance) matrix of \mathcal{G} , $\mathbf{L} \in \mathbb{Z}^{n \times n}$, is a matrix representation of the whole graph, and may be read as a particular case of the discrete Laplace operator. It can be expressed as a combination of the previously defined matrices, as $\mathbf{L} \triangleq \mathbf{D} - \mathbf{A}$, or more interestingly, as:

$$\mathbf{L} \triangleq \mathbf{Q}\mathbf{Q}^T = \mathbf{q}_1\mathbf{q}_1^T + \mathbf{q}_2\mathbf{q}_2^T + \dots + \mathbf{q}_m\mathbf{q}_m^T \quad (12)$$

This allows to formulate the Laplacian as the sum of the effects of each edge,

$$\mathbf{L} \triangleq \sum_{j=1}^m \mathbf{E}_j \quad (13)$$

where the generators $\mathbf{E}_j = \mathbf{q}_j\mathbf{q}_j^T \in \{-1, 0, 1\}^{n \times n}$ represent the connection between a pair of vertices \mathbf{v}_i and \mathbf{v}_k through the edge \mathbf{e}_j . An element of the matrix diagonal is known to be 1 if it is associated to the vertices, i.e. $[E_j]_{i,i}$ and $[E_j]_{k,k}$; and 0 otherwise. Off-diagonal elements are -1 if the nodes are related, i.e. $[E_j]_{i,k}$ and $[E_j]_{k,i}$; and 0 otherwise.

For a weighted graph \mathcal{G}_γ in which edges are defined by $\tilde{\mathbf{e}}_j \triangleq (\mathbf{v}_i, \mathbf{v}_k, \gamma_{i,k})$ with $\gamma_j \equiv \gamma_{i,k} \in \mathbb{R}$, generalization is straightforward. The weighted Laplacian will be now given by:

$$\mathbf{L}_\gamma \triangleq \sum_{j=1}^m \mathbf{E}_j \gamma_j = \begin{cases} -\gamma_{i,k} & \text{if } i \neq k, a_{i,k} = 1 \\ 0 & \text{if } i \neq k, a_{i,k} = 0 \\ \sum_{q=1}^n \gamma_{i,q} & \text{if } i = k \end{cases} \quad (14)$$

Note that the weighted Laplacian is a generalization of the Laplacian and (14) yields to (13) when $\gamma_j = 1 \forall j$. Also, \mathbf{L}_γ is symmetric, positive semi-definite and singular, since it is satisfied that $\mathbf{L}_\gamma \mathbf{1}^T = \mathbf{0}^T$.

D. Spectral Graph Theory

Most important graph connectivity indices come from the analysis of the Laplacian spectrum, since it reflects how a graph is connected. Consider $\boldsymbol{\mu} = (\mu_1, \mu_2, \dots, \mu_n)$ the ordered set of eigenvalues of \mathbf{L} and $\tilde{\boldsymbol{\mu}} = (\tilde{\mu}_1, \tilde{\mu}_2, \dots, \tilde{\mu}_n)$ that of \mathbf{L}_γ ; both ranked in increasing order. In connected graphs, the Laplacian matrix has one zero eigenvalue with unit eigenvector, i.e. $\mu_1 = \tilde{\mu}_1 = 0$.

The simplest metric broadly studied in the literature is the sum of the eigenvalues [31], [32], [33]. The sum of the q -highest eigenvalues, S_q , is known to be bounded by:

$$S_q \leq |\mathcal{E}| + \left\{ \frac{q+1}{2} \right\} \quad (15)$$

where $\left\{ \frac{a}{b} \right\} \triangleq \frac{a!}{b!(a-b)!}$. Equation (15) may be particularized for all the non-zero Laplacian eigenvalues as [31], [33]:

$$S = \sum_{k=2}^n \mu_k = \text{trace}(\mathbf{L}) = \sum_k l_{kk} = 2|\mathcal{E}| = 2m \quad (16)$$

being l_{kk} the diagonal elements of \mathbf{L} .

Since the traces of \mathbf{L} and \mathbf{L}_γ are proportional, as shown hereafter, the previous metric can be easily generalized for a weighted graph.

$$\text{trace}(\mathbf{L}_\gamma) = \sum_{k=1}^n \tilde{\mu}_k = \sum_{k=1}^n \tilde{l}_{kk} = \sum_{j=1}^n \sum_{k=1}^n \gamma_j l_{kk} \quad (17)$$

$$= \frac{1}{n} \sum_{j=1}^n \gamma_j \sum_{k=1}^n l_{kk} = \gamma \sum_{k=1}^n l_{kk} \quad (18)$$

$$\propto \text{trace}(\mathbf{L}) \quad (19)$$

where \tilde{l}_{kk} are the diagonal elements of \mathbf{L}_γ .

A second important index is the number of spanning trees, $t(\mathcal{G})$, that is, the number of sub-graphs that are also trees with minimum number of edges and which set of vertices equals that of the main graph. This index provides a measure for the global reliability of a network. Following Kirchhoff's Matrix-Tree Theorem, it can be obtained using the determinant of the reduced Laplacian matrix, equal to any cofactor of \mathbf{L} :

$$t(\mathcal{G}) \triangleq \det(\mathbf{L}_{\text{reduced}}) = \text{cof}(\mathbf{L}) = \frac{1}{n} \prod_{k=2}^n \mu_k \quad (20)$$

The reduced Laplacian is the matrix obtained after anchoring an arbitrary vertex, i.e., after removing the column and the row associated to that vertex.

The weighted Matrix-Tree Theorem allows to compute the weighted number of spanning trees as:

$$\tilde{t}(\mathcal{G}_\gamma) \triangleq \text{cof}(\mathbf{L}_\gamma) = \frac{1}{n} \prod_{k=2}^n \tilde{\mu}_k \quad (21)$$

The second smallest eigenvalue of the (weighted) Laplacian is also a crucial index of a graph, since its value reflects whether the graph is disconnected [34]. It is known as the algebraic connectivity, or the Fiedler value, and is greater than zero only for connected graphs:

$$\alpha(\mathcal{G}) \triangleq \min(\mu_k : k = 2, \dots, n) = \mu_2 \quad (22)$$

Generalization for weighted graphs is straight-forward.

Finally, the Kirchhoff index, $Kf(\mathcal{G})$, measures the resistance between each pair of vertices under the assumption that edges are unit resistors, and is defined by [35], [36]:

$$Kf(\mathcal{G}) \triangleq n \sum_{k=2}^n \mu_k^{-1} \quad (23)$$

III. A GENERAL RELATIONSHIP BETWEEN OPTIMALITY CRITERIA AND GRAPH CONNECTIVITY INDICES

Consider a typical SLAM pose-graph in which nodes encode robot poses (e.g. key-frames in visual SLAM) and edges encode the relative transformation between node pairs and its uncertainty, usually encoded as a FIM. For the j -th edge, it will be $\Phi_j = \Sigma_j^{-1} \in \mathbb{R}^{\ell \times \ell}$, where ℓ is the dimension of the state vector to be estimated, or the number of degrees of freedom of the space with dimension n' ; that is, $\ell = n'(n' + 1)/2$.

In general, the state vector in SLAM, \mathbf{x}_i , contains the position and orientation of the robot/sensor at a certain time. Using the special Euclidean group, $SE(n')$, the robot's pose and its uncertainty can be defined with Lie groups. As in differential representations, the real location of the robot w.r.t. a global frame (w), \mathbf{T}_{wi} , is defined by a large noise-free value which contains the estimated location, and a small (differential) perturbation that fully encodes the estimation error. That is,

$$\mathbf{T}_{wi} = \bar{\mathbf{T}}_{wi} \exp(\hat{\mathbf{d}}_i) \quad (24)$$

where $\bar{\mathbf{T}}_{wi} \in SE(n')$ is the i -th estimation, and $\mathbf{d}_i \equiv \mathbf{d}_{ii} \in \mathbb{R}^\ell$ is a random vector normally distributed and defined by its mean $\bar{\mathbf{d}}_i = \mathbb{E}[\mathbf{d}_i]$ and covariance $\Sigma_j = \mathbb{E}[(\mathbf{d}_i - \bar{\mathbf{d}}_i)(\mathbf{d}_i - \bar{\mathbf{d}}_i)^T]$; expressed in its own frame (i). This vector is usually represented by $(dx, dy, d\theta)^T$ and $(dx, dy, dz, d\omega_x, d\omega_y, d\omega_z)^T$ for the 2D and 3D cases, respectively. Note that the hat operator defines the mapping $\hat{\cdot} : \mathbb{R}^\ell \rightarrow \mathbf{H} \in \mathbb{R}^{(n'+1) \times (n'+1)}$, i.e. it maps elements from the real vector space to that of the Lie algebra $\mathfrak{se}(n')$. See Appendix A for more details on notation and formulation of Lie groups.

Equivalently, the estimation error can be expressed in the global frame, as it might also be done in differential representations [37]. In this case, the matrix exponential will precede the robot's location estimate:

$$\mathbf{T}_{wi} = \exp(\hat{\mathbf{d}}_{wi}) \bar{\mathbf{T}}_{wi} \quad (25)$$

Both uncertainty perturbation variables, \mathbf{d}_i and \mathbf{d}_{wi} , are related by the adjoint action of the Lie group, a way of representing the elements of the group as linear transformations of the group's Lie algebra. That is, it transforms a vector from the tangent space around one element to that of another. Therefore,

$$\mathbf{d}_i = Ad_{\bar{\mathbf{T}}_{iw}} \mathbf{d}_{wi} \Leftrightarrow \mathbf{d}_{wi} = Ad_{\mathbf{T}_{wi}} \mathbf{d}_i \quad (26)$$

where $Ad_{\bar{\mathbf{T}}_{wi}}$ is the adjoint representation of $\bar{\mathbf{T}}_{wi}$ and is defined, in $SE(2)$ and $SE(3)$ respectively, as,

$$Ad_{\bar{\mathbf{T}}_{wi}} = \left(\begin{array}{c|c} \mathbf{R}_{wi} & \mathbf{R}_{wi} \begin{pmatrix} y_{wi} \\ -x_{wi} \end{pmatrix} \\ \hline \mathbf{0} & 1 \end{array} \right) \quad (27)$$

$$Ad_{\mathbf{T}_{wi}} = \left(\begin{array}{c|c} \mathbf{R}_{wi} & [\mathbf{p}_{wi}]_{\times} \mathbf{R}_{wi} \\ \hline \mathbf{0} & \mathbf{R}_{wi} \end{array} \right) \quad (28)$$

where $\mathbf{R}_{wi} \in SO(n')$ is the orthogonal matrix that encodes the rotation part of \mathbf{T}_{wi} , and $[\mathbf{p}_{wi}]_{\times} \in \mathbb{R}^{3 \times 3}$ is the skew symmetric matrix related to the translational part of \mathbf{T}_{wi} for 3D. See Appendix A.

Consider now two noisy poses \mathbf{T}_{wi} and \mathbf{T}_{wk} . The relative transformation between them will be given by:

$$\mathbf{T}_{ik} = \mathbf{T}_{wi}^{-1} \mathbf{T}_{wk} \quad (29)$$

$$= \bar{\mathbf{T}}_{wi}^{-1} \exp(\hat{\mathbf{d}}_{wi})^{-1} \exp(\hat{\mathbf{d}}_{wk}) \bar{\mathbf{T}}_{wk} \quad (30)$$

Using the following definition of the adjoint:

$$\exp(Ad_{\mathbf{A}} \mathbf{B}) \triangleq \mathbf{A} \exp(\mathbf{B}) \mathbf{A}^{-1} \quad (31)$$

with $\mathbf{A} = \bar{\mathbf{T}}_{wi}^{-1}$ and $\mathbf{B} = \hat{\mathbf{d}}_{wi}$, (30) becomes:

$$\mathbf{T}_{ik} = \exp(-Ad_{\bar{\mathbf{T}}_{wi}^{-1}} \hat{\mathbf{d}}_{wi}) \exp(Ad_{\bar{\mathbf{T}}_{wi}^{-1}} \hat{\mathbf{d}}_{wk}) \bar{\mathbf{T}}_{wi}^{-1} \bar{\mathbf{T}}_{wk} \quad (32)$$

Finally, using the first-order approximation [38] of the Baker-Campbell-Hausdorff formula for the product of exponential maps,

$$\mathbf{T}_{ik} \simeq \exp(-Ad_{\bar{\mathbf{T}}_{wi}^{-1}} \hat{\mathbf{d}}_{wi} + Ad_{\bar{\mathbf{T}}_{wi}^{-1}} \hat{\mathbf{d}}_{wk}) \bar{\mathbf{T}}_{wi}^{-1} \bar{\mathbf{T}}_{wk} \quad (33)$$

$$= \exp(\hat{\mathbf{d}}_{ik}) \bar{\mathbf{T}}_{ik} \quad (34)$$

The estimation error of the composed pose can be expressed in the common reference frame and in the real vector space as follows:

$$\mathbf{d}_{ik}^w \simeq Ad_{\bar{\mathbf{T}}_{wi}} Ad_{\bar{\mathbf{T}}_{wi}^{-1}} (-\mathbf{d}_{wi} + \mathbf{d}_{wk}) \quad (35)$$

$$= -\mathbf{d}_{wi} + \mathbf{d}_{wk} \quad (36)$$

$$= (-\mathbf{I}_{\ell \times \ell} \quad \mathbf{I}_{\ell \times \ell}) \begin{pmatrix} \mathbf{d}_{wi} \\ \mathbf{d}_{wk} \end{pmatrix} \quad (37)$$

with $\mathbf{I}_{\ell \times \ell}$ the identity matrix of size ℓ .

Equation (37) can be generalized for a complete pose-graph containing every robot pose in the trajectory. In that case, the random vector associated to the estimation error between two arbitrary vertices (i, k) related through the j -th edge will be given by:

$$\mathbf{d}_j \equiv \mathbf{d}_{ik}^w \simeq \begin{pmatrix} \mathbf{0} \\ \vdots \\ -\mathbf{I}_{\ell \times \ell} \\ \vdots \\ \mathbf{I}_{\ell \times \ell} \\ \vdots \\ \mathbf{0} \end{pmatrix}^T \begin{pmatrix} \mathbf{d}_{w1} \\ \vdots \\ \mathbf{d}_{wi} \\ \vdots \\ \mathbf{d}_{wk} \\ \vdots \\ \mathbf{d}_{wn} \end{pmatrix} = \mathcal{I}_j \delta_w \quad (38)$$

where \mathcal{I}_j is the 1-by- n block matrix populated with zero matrices everywhere but in $[\mathcal{I}_j]_{1,k} = -[\mathcal{I}_j]_{1,i} = \mathbf{I}_{\ell \times \ell}$.

Revisiting (1), ML approaches aim to find the set of poses that minimize the constraints introduced either by odometry or loop closures. Using (38), the cost function of an arbitrary

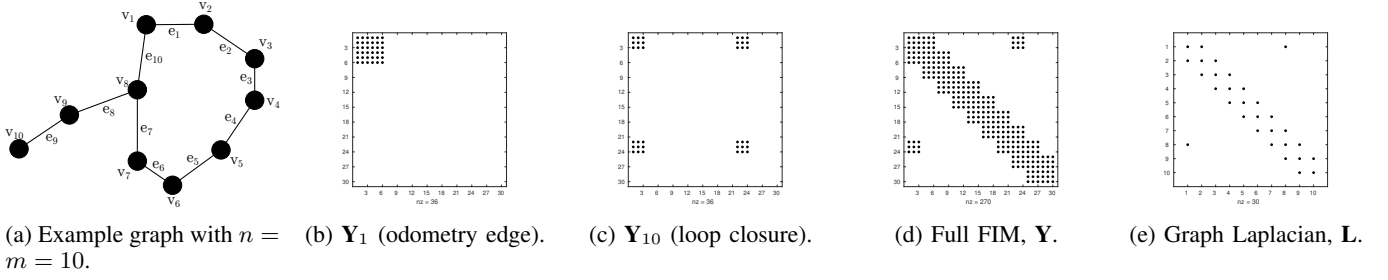


Fig. 1: Example of the generators \mathbf{Y}_j and the full FIM \mathbf{Y} for an example 2D pose-graph with $n = m = 10$, including one loop closure. In images (b) to (d), non-zero matrix elements are depicted with black dots. Also, the Laplacian of the graph is shown in figure (e).

edge may be rewritten as a function of all known estimation errors:

$$\mathbf{F}_j \simeq \delta_w^T \mathcal{I}_j^T \Sigma_j^{-1} \mathcal{I}_j \delta_w \quad (39)$$

$$= \delta_w^T \underbrace{\begin{pmatrix} \ddots & & & & \\ & \Sigma_j^{-1} & \cdots & -\Sigma_j^{-1} & \\ \vdots & \vdots & \ddots & \vdots & \vdots \\ & -\Sigma_j^{-1} & \cdots & \Sigma_j^{-1} & \\ \cdot & \cdot & \cdot & \cdot & \ddots \end{pmatrix}}_{\mathbf{Y}_j} \delta_w \quad (40)$$

where the symmetric matrix $\mathbf{Y}_j \in \mathbb{R}^{n\ell \times n\ell}$ is the information matrix of the full graph associated to the j -th edge and n the number of nodes of the graph. Every block element in this matrix will be zero except for those associated to the vertices related by that edge, which will be Φ_j if they are in the diagonal and $-\Phi_j$ otherwise. Note that the matrix dimensions will grow as the robot moves. Interestingly, using the Kronecker product (see definition and properties in Appendix B), it can be expressed in terms of the topology of the underlying graph as:

$$\mathbf{Y}_j = \mathcal{I}_j^T \Sigma_j^{-1} \mathcal{I}_j = \mathbf{E}_j \otimes \Sigma_j^{-1} \quad (41)$$

Finally, the FIM of the whole system (sum of the contributions of each edge) can be expressed as:

$$\therefore \mathbf{Y} = \sum_{j=1}^m \mathbf{Y}_j = \sum_{j=1}^m \mathbf{E}_j \otimes \Sigma_j^{-1} \quad (42)$$

Again, $\mathbf{Y} \in \mathbb{R}^{n\ell \times n\ell}$ will be a block matrix populated with $\mathbf{0}$ and $\pm\Phi_j$ sub-matrices. Note that this formulation over Lie groups is analogous to the differential one (see, e.g., [2]), although here the equivalent measurement Jacobian would be embedded in δ_w instead of in \mathbf{Y}_j .

Figure 1 contains an illustrative example of the computation of \mathbf{Y} , two of its generators and the Laplacian of the underlying graph, \mathbf{L} , for a toy graph with $n = m = 10$. The similarity in the (sparsity) block patterns of the graph's information matrix and the Laplacian can be seen in images 1d and 1e.

Two special cases of equation (42) arise, in which it is possible to directly relate the full information matrix to the graph Laplacian (14). The first one corresponds to the situation where the covariance matrix is constant through

measurements; a common assumption in related literature [22], although rarely represents reality and is consistent only during exploratory trajectories. Under this hypothesis, by leveraging the associative property of the Kronecker product (see Appendix B), (42) becomes:

$$\mathbf{Y} = \sum_{j=1}^m \mathbf{E}_j \otimes \bar{\Sigma}^{-1} = \mathbf{L} \otimes \bar{\Sigma}^{-1} \quad \text{if } \Sigma_j = \bar{\Sigma} \forall j \quad (43)$$

with $\bar{\Sigma}$ constant.

The second case considers the information matrix to have an upper bound for every edge in the trajectory, that is,

$$\mathbf{Y}_j = \mathbf{E}_j \otimes \Sigma_j^{-1} \preceq \mathbf{Y}_{j,upper} \quad \forall j \quad (44)$$

where $\mathbf{A} \succeq \mathbf{B}$ means $\mathbf{A} - \mathbf{B}$ is positive semi-definite. This bound can be defined for every edge by considering $\mathbf{Y}_{j,upper} = \mathbf{E}_j \otimes \Sigma_{j,upper}^{-1}$ and a lower bound in the covariance matrices, that is:

$$\Sigma_j \succeq \beta_j \bar{\Sigma} \Leftrightarrow \Sigma_j^{-1} \preceq \Sigma_{j,upper}^{-1} = \alpha_j \bar{\Sigma}^{-1} \quad (45)$$

with $0 < \beta_j \leq 1$ and $\alpha_j \geq 1$. This guess would make β_j to increase during exploratory trajectories and decrease, for example, when a loop is closed. A lower bound on the covariance matrix could be helpful to evaluate the usefulness of loop closures and compare two possible trajectories (*exploration-exploitation dilemma*). On the other hand, an upper bound could be useful to know when information gain is too low to continue exploration and hence to decide when to stop it.

One smart and mathematically-consistent way to establish the upper bound for Φ_j is through its eigenvalues, since any positive semi-definite matrix can be considered trivially upper-bounded by a diagonal matrix with its largest eigenvalue as diagonal terms. Let $(\lambda_1^j, \dots, \lambda_\ell^j)$ be the ordered set of eigenvalues of Σ_j , ranked in increasing order, and $(\rho_1^j, \dots, \rho_\ell^j) = \left(\frac{1}{\lambda_\ell^j}, \dots, \frac{1}{\lambda_1^j}\right)$ that of Φ_j . Then, the bound in (45) can be expressed in terms of the eigenvalues of the covariance matrix of each edge as:

$$\Sigma_j \succeq \lambda_1^j \mathbf{I}_{\ell \times \ell} \Leftrightarrow \Sigma_j^{-1} \preceq \rho_\ell^j \mathbf{I}_{\ell \times \ell} = \frac{1}{\lambda_1^j} \mathbf{I}_{\ell \times \ell} \quad (46)$$

Using the previous bound and the associative property of the Kronecker product, (42) can be particularized to:

$$\mathbf{Y} \preceq \sum_{j=1}^m \left(\rho_\ell^j \mathbf{E}_j \right) \otimes \bar{\Sigma}^{-1} \quad (47)$$

$$= \mathbf{L}_\gamma \otimes \bar{\Sigma}^{-1} \quad \text{if } \Sigma_j^{-1} \preceq \rho_\ell^j \bar{\Sigma}^{-1} \quad \forall j \quad (48)$$

where \mathbf{L}_γ is the Laplacian of the graph in which each edge is weighted with $\gamma_j = \rho_\ell^j$. Note that the previous equation yields to (43) for the case that $\gamma_j = 1 \quad \forall j$.

A. On the Spectra

Consider now $(\bar{\rho}_1, \dots, \bar{\rho}_\ell)$ to be the ordered set of eigenvalues of $\bar{\Phi} = \bar{\Sigma}^{-1}$, and $(0 = \mu_1, \mu_2, \dots, \mu_n)$ that of the Laplacian matrix \mathbf{L} , again ranked in increasing order. According to the spectral properties of the Kronecker product (see proof in Appendix B):

$$\text{eig}(\mathbf{L} \otimes \bar{\Sigma}^{-1}) = \mu_k \bar{\rho}_b, \quad \begin{matrix} k = 1, \dots, n \\ b = 1, \dots, \ell \end{matrix} \quad (49)$$

Therefore, and while under assumption of constant covariance, it can be stated that any utility function applied to the graph information matrix may be found by applying it separately to the Laplacian (after removing its zero eigenvalue, i.e. reduced Laplacian) and to the FIM associated to the graph's edges, which will be constant and greater than zero. That is,

$$\|\mathbf{Y}\|_p = \begin{cases} \|\mathbf{L}\|_p \|\bar{\Sigma}^{-1}\|_p & \text{if } 0 < |p| < \infty \\ \|\mathbf{L}\|_p \|\bar{\Sigma}^{-1}\|_p \|\bar{\Sigma}^{-1}\|_p^{-\frac{1}{n}} & \text{if } p = 0 \end{cases} \quad (50)$$

Or, equivalently,

$$\therefore \|\mathbf{Y}\|_p \propto \|\mathbf{L}\|_p \equiv \|\mathbf{L}_{\gamma=1}\|_p \quad \forall p \quad (51)$$

Proof: For $0 < |p| < \infty$,

$$\|\mathbf{Y}\|_p = \left(\frac{1}{n\ell} \sum_{k=2}^n \sum_{b=1}^\ell (\mu_k \bar{\rho}_b)^p \right)^{\frac{1}{p}} \quad (52)$$

$$= \left(\frac{1}{n\ell} \sum_{k=2}^n \mu_k^p \sum_{b=1}^\ell \bar{\rho}_b^p \right)^{\frac{1}{p}} \quad (53)$$

$$= \left(\frac{1}{n} \sum_{k=2}^n \mu_k^p \right)^{\frac{1}{p}} \left(\frac{1}{\ell} \sum_{b=1}^\ell \bar{\rho}_b^p \right)^{\frac{1}{p}} \quad (54)$$

$$= \|\mathbf{L}\|_p \|\bar{\Sigma}^{-1}\|_p \quad (55)$$

and for $p = 0$,

$$\|\mathbf{Y}\|_p = \exp \left[\frac{1}{n\ell} \sum_{k=2}^n \sum_{b=1}^\ell \log(\mu_k \bar{\rho}_b) \right] \quad (56)$$

$$= \exp \left[\frac{1}{n\ell} \left(\ell \sum_{k=2}^n \log(\mu_k) + (n-1) \sum_{b=1}^\ell \log(\bar{\rho}_b) \right) \right] \quad (57)$$

$$= \exp \left[\frac{1}{n} \sum_{k=2}^n \log(\mu_k) + \frac{n-1}{n\ell} \sum_{b=1}^\ell \log(\bar{\rho}_b) \right] \quad (58)$$

$$= \exp \left[\frac{1}{n} \sum_{k=2}^n \log(\mu_k) \right] \exp \left[\frac{1}{\ell} \sum_{b=1}^\ell \log(\bar{\rho}_b) \right]^{1-\frac{1}{n}} \quad (59)$$

$$= \|\mathbf{L}\|_p \|\bar{\Sigma}^{-1}\|_p \|\bar{\Sigma}^{-1}\|_p^{-\frac{1}{n}} \quad (60)$$

Note that in all cases the zero eigenvalue of the Laplacian has been removed, equivalent to anchoring an arbitrary vertex. ■

Similarly, the following inequality is satisfied for the case all measurements are bounded as expressed in (48):

$$\therefore \|\mathbf{Y}\|_p \leq \|\mathbf{L}_\gamma\|_p \quad \forall p \quad (61)$$

being \mathbf{L}_γ the Laplacian matrix of the graph weighted with $\gamma_j = \rho_\ell^j = \|\Phi_j\|_\infty = \tilde{E}\text{-opt}(\Phi_j)$.

Proof: Since \mathbf{Y} and \mathbf{L}_γ are symmetric, positive semi-definite and $\mathbf{Y} \preceq \mathbf{L}_\gamma \otimes \mathbf{I}_{\ell \times \ell}$ (48), then (Weyl's Monotonicity Theorem [39, p. 26]):

$$\|\mathbf{Y}\|_p \leq \|\mathbf{L}_\gamma \otimes \mathbf{I}_{\ell \times \ell}\|_p \quad (62)$$

For $0 < |p| < \infty$,

$$\|\mathbf{Y}\|_p \leq \left(\frac{1}{n\ell} \sum_{k=2}^n \sum_{b=1}^\ell (\tilde{\mu}_k 1)^p \right)^{\frac{1}{p}} \quad (63)$$

$$= \left(\frac{1}{n} \sum_{k=2}^n \tilde{\mu}_k^p \right)^{\frac{1}{p}} = \|\mathbf{L}_\gamma\|_p \quad (64)$$

and for $p = 0$,

$$\|\mathbf{Y}\|_p = \exp \left[\frac{1}{n\ell} \sum_{k=2}^n \sum_{b=1}^\ell \log(\tilde{\mu}_k 1) \right] \quad (65)$$

$$= \exp \left[\frac{1}{n\ell} \ell \sum_{k=2}^n \log(\tilde{\mu}_k) \right] = \|\mathbf{L}_\gamma\|_p \quad (66)$$

where $(\tilde{\mu}_1, \tilde{\mu}_2, \dots, \tilde{\mu}_n)$ are the eigenvalues of \mathbf{L}_γ . ■

Expressions in both (51) and (61) allow to shift the traditional approach of applying utility functions to \mathbf{Y} , to a new strategy where they are applied to \mathbf{L}_γ . Given that new optimality criteria will be functionals of the eigenvalues of the reduced (weighted) Laplacian, the Spectral Graph Theory presented in Section II-D can be leveraged.

Therefore, and only under the assumption that every measurement has the same covariance, optimality criteria of \mathbf{Y} (and equivalently that of Σ , see Appendix C) can be expressed in terms of the graph's structure as:

$$T\text{-opt}(\mathbf{Y}) = A\text{-opt}(\Sigma)^{-1} \propto \bar{d} \quad (67)$$

$$D\text{-opt}(\mathbf{Y}) = D\text{-opt}(\Sigma)^{-1} \propto (n \, t(\mathcal{G}))^{\frac{1}{n}} \quad (68)$$

$$A\text{-opt}(\mathbf{Y}) = T\text{-opt}(\Sigma)^{-1} \propto \frac{n^2}{Kf(\mathcal{G})} \quad (69)$$

$$E\text{-opt}(\mathbf{Y}) = \tilde{E}\text{-opt}(\Sigma)^{-1} \propto \alpha(\mathcal{G}) \quad (70)$$

where $\bar{d} \triangleq 2m/n$ is known as the average degree of the graph. Note that these results are consistent with those reported in [22] for the particular case they studied in which $\ell = \{2, 3\}$, covariance is constant through measurements and $D\text{-opt}$ is defined in a traditional way [40].

For the more general case of bounded uncertainty, they become:

$$T\text{-opt}(\mathbf{Y}) = A\text{-opt}(\Sigma)^{-1} \leq \bar{d} \bar{\gamma} \quad (71)$$

$$D\text{-opt}(\mathbf{Y}) = D\text{-opt}(\Sigma)^{-1} \leq (n \tilde{t}(\mathcal{G}_\gamma))^{\frac{1}{n}} \quad (72)$$

$$A\text{-opt}(\mathbf{Y}) = T\text{-opt}(\Sigma)^{-1} \leq (*) \quad (73)$$

$$E\text{-opt}(\mathbf{Y}) = \tilde{E}\text{-opt}(\Sigma)^{-1} \leq \tilde{\alpha}(\mathcal{G}_\gamma) \quad (74)$$

where \mathcal{G}_γ now denotes the pose-graph weighted with $\gamma_j = \tilde{E}\text{-opt}(\Phi_j)$.

Note that (73), dependent of the Kirchhoff index of the weighted graph, is not complete due to the complexity on its calculation. Also, computation of the Laplacian determinant to evaluate the number of spanning trees quickly becomes intractable for large graphs, as well as it generates low precision for small values. Using the logarithmic determinant avoids under and overflow. Thus, (72) may be efficiently computed via:

$$D\text{-opt}(\mathbf{Y}) \leq n^{\frac{1}{n}} \exp \{ \log(\tilde{t}(\mathcal{G}_\gamma))/n \} \quad (75)$$

IV. EXPERIMENTAL VALIDATION

In this section, we show several experiments in order to prove the theoretical relationships proposed in (67)-(74) hold. Datasets from [41] and [42], which are publicly available², have been used for 2D and 3D experiments, respectively. Every sequence in the datasets contains a pose-graph, either on *g2o* or *toro* format. They have been optimized using Ceres as if it were a global bundle adjustment at the end of the sequence. Each of them contains the following information after pre-processing:

- Nodes: id., absolute pose.
- Edges: id. 1, id. 2, type of constraint (odometry, loop closure), relative transformation, FIM associated to it.

To compare both approaches, we simulate the construction of the pose-graph as if the robot were performing active SLAM. That is, at each time step a new node with its corresponding constraints is added to the graph and optimality criteria is computed using both \mathbf{Y} and \mathbf{L} . All experiments have been performed on an Intel Core i9-10900K CPU @ 3.70GHz.

A. Constant Uncertainty along Edges

Firstly, we consider uncertainty to be constant along the trajectory like in the first hypothesis of the previous section. Suppose the standard deviations of the linear movement to be $\sigma_x = 0.3$ m and $\sigma_y = 0.4$ m, and that of the orientation $\sigma_\theta = 0.063$ rad. If we only consider X and Y cross-correlated with Pearson correlation coefficient 0.36, the information matrix of any edge will be:

$$\Phi_j = \bar{\Phi} = \begin{pmatrix} 11.11 & -3 & 0 \\ -3 & 6.25 & 0 \\ 0 & 0 & 250 \end{pmatrix} \quad \forall j \quad (76)$$

We used a reduced trajectory of the Freiburg University Hospital (FRH) dataset, assigning the previous information matrix to every edge. Figure 2 shows the complete (black)

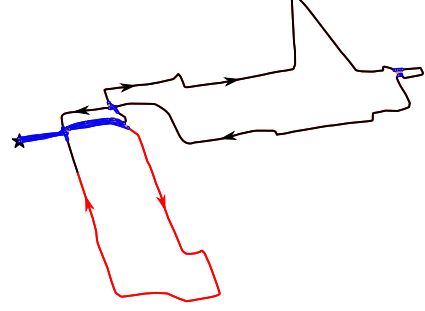


Fig. 2: Complete (black) and reduced (red) trajectories of the FRH dataset, where loop closures are depicted with blue dots.

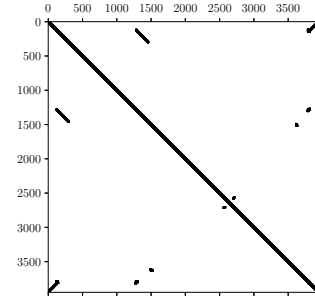


Fig. 3: Sparsity pattern of the full FIM in the FRH dataset.

and reduced (red) trajectories of this sequence, that consists of 1316 nodes and 1485 constraints (thus 170 corresponding to loop closures). The reduced trajectory is purely exploratory and contains the path before the first loop closure occurs. Also, this figure contains the loop closure constraints (blue dots), which can be also spotted in the sparsity pattern of the full FIM in Figure 3.

Figure 4 shows the computed T -, D -, A - and E -opt using the estimation-theoretic (blue) and graphical (red curves) facets of the problem. All curves overlap, proving that the relationships in (67)-(70) hold, and, moreover, that the proportionality constants derived in (50) are consistent.

Time consumed by both approaches per step appears in Fig. 5, clearly showing the advantage of computing $\|\mathbf{L}\|_p \|\bar{\Phi}\|_p$ (red) over $\|\mathbf{Y}\|_p$ (blue curve) as the pose-graph grows. Studying computational complexity, it is easy to notice that computing optimality criteria on \mathbf{L} requires $\mathcal{O}(n^3) + \mathcal{O}(\ell^3)$ while applying them to \mathbf{Y} requires $\mathcal{O}(\ell^3 n^3)$, omitting lower order terms, being $\mathcal{O}(\cdot)$ a lower bound, n the number of nodes in the graph and ℓ the dimension of the state vector (3 for this dataset). Also, as the FIM dimensions grow, building \mathbf{Y} requires way far more resources than creating \mathcal{G} .

The same analysis can be done when edges share a constant covariance matrix, $\Sigma_j = \bar{\Sigma} = \bar{\Phi}^{-1} \forall j$, with the subtle difference that (51) now becomes (see Appendix C):

$$\|\Sigma\|_p = \|\mathbf{Y}^{-1}\|_p \propto \|\mathbf{L}^{-1}\|_p = (\|\mathbf{L}\|_{-p})^{-1} \quad (77)$$

Appendix D contains the results for optimality criteria of the covariance matrix in the same trajectory of FRH dataset.

²<https://lucacarlone.mit.edu/datasets/>

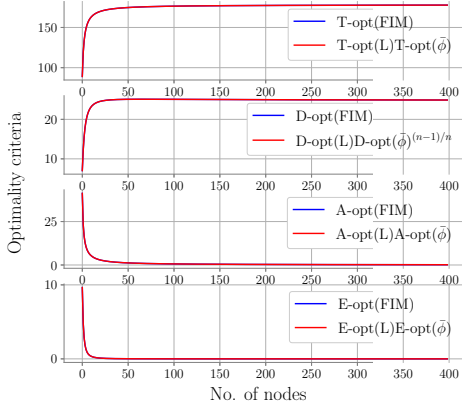


Fig. 4: Optimalty criteria of the information matrix (blue) and the Laplacian (red), for the reduced FRH dataset.

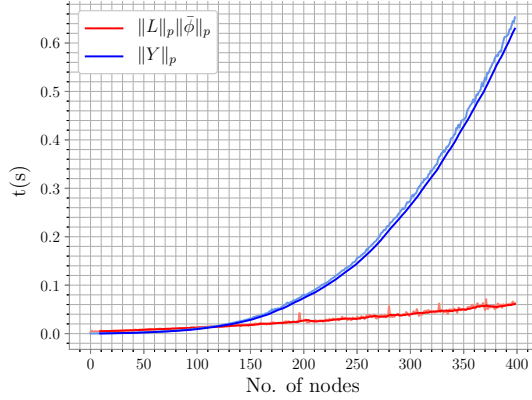


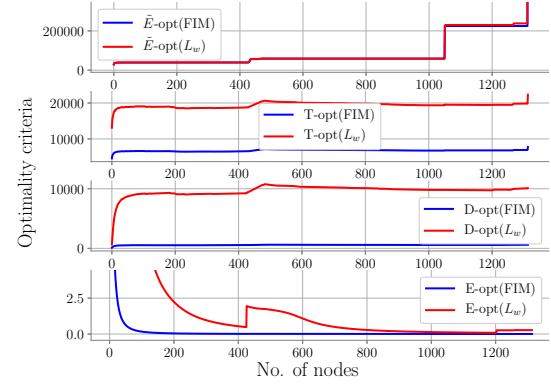
Fig. 5: Time required at each step (in seconds) to compute optimality criteria of both approaches; for the reduced FRH dataset.

B. Variable Uncertainty along Edges

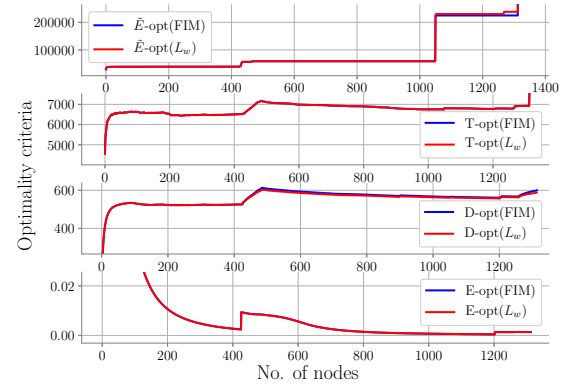
Consider now the second and more realistic case in which edges' information matrices are no longer constant. According to (46) and (61), one needs to build a graph weighted with $\gamma_j = \hat{E}\text{-opt}(\Phi_j)$.

In this case, the whole trajectory contained in FRH dataset has been used with the original information matrices, inasmuch as it is tractable despite being computationally intensive. Figure 6a contains the resulting \hat{E} -, T -, D - and E -opt for both the information matrix (blue) and the weighted Laplacian (red curves). The selected bound indeed limits $\|Y\|_p \forall p$, though it is an extremely conservative one. Since $\hat{E} - \text{opt} \geq T - \text{opt} \geq D - \text{opt} \geq A - \text{opt} \geq E - \text{opt}$, the upper limit does hold for every criteria. But more interestingly, it makes $\hat{E} - \text{opt}(Y)$ and $\hat{E} - \text{opt}(L_\gamma)$ to be approximately equal during the whole trajectory. This brings about the idea that using the same optimality criterion to be estimated as weights would result in more accurate approximations. The bound in (46) can be replaced by:

$$\Phi_j \approx \|\Phi_j\|_p \mathbf{I}_{\ell \times \ell} \quad (78)$$



(a) $\gamma_j = \|\Phi_j\|_\infty$.



(b) $\gamma_j = \|\Phi_j\|_p$.

Fig. 6: Optimalty criteria of the information matrix (blue) and the Laplacian (red) in FRH dataset, weighted with (a) $\|\Phi_j\|_\infty$, and (b) $\|\Phi_j\|_p$.

Which leads to the following approximation relationship,

$$\|Y\|_p \approx \|L_\gamma\|_p \text{ with } \gamma_j = \|\Phi_j\|_p \forall p \quad (79)$$

Figure 6b shows the results in the same dataset using the new weights. It is easy to notice how blue and red curves are now much closer to each other, even overlapping during certain parts of the trajectory. The trend of red curves is just the same as in Figure 6a, but in this case the scale factor w.r.t. the blue ones is significantly lower. Interestingly, during the beginning of the trajectory, they are exactly the same since all those exploratory edges have approximately the same information in the original dataset (constant uncertainty case).

Further experiments have been carried out using the MIT Killian Court, the Intel Research Lab and the 3D Parking Garage datasets; to prove the proposed relationships hold and that are not dependent on the dimension of the estimation vector. Analogous results to those seen in FRH dataset have been obtained, and they are explained and presented in Appendix D.

Since it is hard to capture the exact difference between blue and red curves in the figures presented, Table I contains the median percentage errors when using our approximations

Dataset				Approximation Error				Time		
	n	m	d	$\Delta\tilde{E}\text{-opt}$	$\Delta T\text{-opt}$	$\Delta D\text{-opt}$	$\Delta E\text{-opt}$	$t(\ \mathbf{Y}\ _p)$	$t(\ \mathbf{L}_\gamma\ _p)$	Δt
MIT	807	827	2.1	2.76%	$\sim 0\%$	0.16%	3.53%	13.75	1.96	85.7%
FR079	989	1217	2.4	0.43%	$\sim 0\%$	7.15%	5.33%	26.50	3.07	88.4%
CSAIL	1045	1171	2.2	0.11%	$\sim 0\%$	1.68%	1.05%	33.90	2.73	91.9%
INTEL	1227	1481	2.4	$\sim 0\%$	$\sim 0\%$	5.85%	7.19%	63.29	7.46	88.2%
FRH	1316	1485	2.2	$\sim 0\%$	$\sim 0\%$	0.76%	0.49%	121.77	5.42	95.6%
MH01 (monocular)	376	544	2.9	$\sim 0\%$	$\sim 0\%$	0.74%	1.49%	4.22	0.56	86.6%
V101 (monocular)	264	415	3.1	$\sim 0\%$	$\sim 0\%$	0.13%	3.27%	1.01	0.14	84.9%
V101-103 (stereo-multi)	322	369	2.3	$\sim 0\%$	$\sim 0\%$	0.40%	3.65%	2.21	0.30	86.1%
V201 (stereo-inertial)	337	598	3.5	$\sim 0\%$	$\sim 0\%$	0.79%	0.05%	2.65	0.16	94.0%
Garage	1661	2615	3.1	0.01%	$\sim 0\%$	6.21%	7.55%	1549.9	11.70	99.2%
Mean	-	-	-	0.34%	$\sim 0\%$	2.38%	3.36%	-	-	90.1%

TABLE I: Percentage error (median) in estimation of optimality criteria using the graph Laplacian instead of the full FIM. Also, the accumulated time required to compute both approaches (in minutes) and the time reduction achieved.

instead of the computations over \mathbf{Y} . It contains the results for all the previously mentioned datasets, but also for Freiburg Building 079 and MIT CSAIL building datasets (2D), and for some EuRoC sequences (3D) [43]. In order to analyze the underlying pose-graph in the latter, they have been processed with ORB-SLAM3 [44]: MH01 and V101 in monocular mode, V202 in stereo inertial, and V101 to V103 in stereo multi-map.

Quantitative results denote that differences between computing $\|\mathbf{L}_\gamma\|_p$ and $\|\mathbf{Y}\|_p$ are indeed very low, and even indistinguishable in some cases. It is crucial to note that, regardless of the absolute error values, the uncertainty trend is always maintained; a key aspect for the use of this approach in active SLAM. The goodness of the estimation highly depends (i) on the number of off-diagonal elements in both Φ_j (cross-correlations) and \mathbf{Y} (loop closures); (ii) on the values of the off-diagonal terms in Φ_j , relative to those in the main diagonal; and (iii) on how every criterion accounts for them. For instance, $T\text{-opt}$ was perfectly computed in all cases, showing (numerical) errors in the order of 10^{-6} or less. This criterion computes the trace of the matrix, so elements outside the main diagonal of both Φ_j and \mathbf{Y} are neglected. The case of $\tilde{E}\text{-opt}$ is akin (0.3% error on average), since the highest eigenvalue is weakly affected by elements outside the main diagonal when they are lower than those on it. Moreover, since this criterion overestimates the information matrices, $\tilde{E}\text{-opt}(\mathbf{L}_w) \gtrsim \tilde{E}\text{-opt}(\mathbf{Y})$ holds. See, e.g., first subplot in Figure 6b. The smallest eigenvalue, however, is more sensitive to off-diagonal terms, even when they are small. Estimation error of $E\text{-opt}$ is higher (3.4%), also due to the numerical complexity of precisely computing the smallest eigenvalue of high-dimensional matrices. In contrast to the previous criterion, it holds that $E\text{-opt}(\mathbf{L}_w) \lesssim E\text{-opt}(\mathbf{Y})$. $D\text{-opt}$ subtly inherited that behavior since it takes into account all eigenvalues, showing 2.4% approximation error, on average. A deeper analysis of the results showed that $\Delta\tilde{E}\text{-opt}$, $\Delta D\text{-opt}$ and $\Delta E\text{-opt}$ slightly increase as the amount of loop closure constraints do. On the other hand, density of the edge's information matrices slightly affects $\Delta\tilde{E}\text{-opt}$ and $\Delta D\text{-opt}$ but strongly alters $\Delta E\text{-opt}$. This occurred in some sequences in which Φ_j are dense $\forall j$ and absolute values of the off-diagonal

terms are close to those in the main diagonal.

In addition, Table I contains the total time required to compute all criteria with both approaches (in minutes) and the percentage of reduction achieved using the graph Laplacian. These computations require, in one case: (a) building the full FIM and (b) computing optimality criteria; and in the other case: (a) building 4 different sub-graphs, (b) analyzing their connectivity indices and (c) computing optimality criteria equivalences. Note that results comprise the computation of four of the modern optimality criteria presented in Section II-B, and therefore computation of all eigenvalues is required. In order to make a fair comparison, both methods are evaluated under the same conditions, and eigenvalues are computed leveraging fast decomposition for real-symmetric matrices. Matrices were not assumed sparse, since it was detrimental for \mathbf{Y} in some datasets.

To sum up, in just 10% of the time that traditional computations over the FIM would require, optimality criteria of the weighted Laplacian yield approximations that maintain the same trend and have 2% error, on average.

V. ONLINE D-OPTIMALITY ACTIVE SLAM

Sections III and IV have proven, both theoretically and experimentally, that analyzing the connectivity of the underlying graph, weighted with the same criterion to be computed, is equivalent to analyzing optimality criteria over \mathbf{Y} in order to perform active SLAM; with the difference of significantly lower computing time. In this section, we take a further step in this direction, tackling the problem of executing online D -optimal active SLAM. Figure 7 shows an overview of the designed system, in which active SLAM is performed in Gazebo simulator, within a ROS Noetic framework.

Our approach contains two main parts. The first one (SLAM) deals with the estimation of the robot's pose and the building of a map of the environment from raw laser measurements, using a modified version of Karto-SLAM. It uses Open Karto [45] for graph construction (front-end) and $g2o$ [46] for graph optimization (back-end). This SLAM algorithm builds an occupancy grid with 5 cm resolution. Other relevant parameters are: minimum travel distance and heading

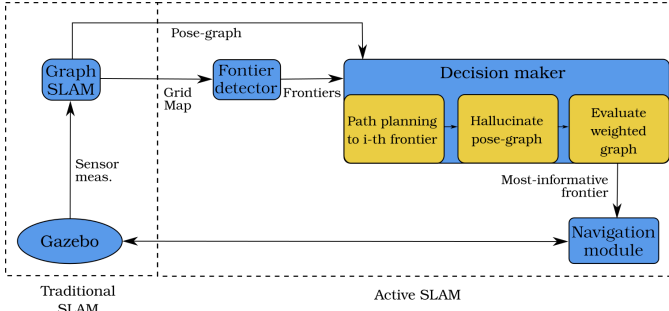


Fig. 7: Overview of the proposed active SLAM system.

of 0.3 m and 0.3 rad, respectively, minimum search distance of 6 m, and search space dimension and resolution of 4 m and 8 cm, respectively. Graph optimization uses Gauss Newton algorithm. On the other hand, the second module, which originates from [29], handles the three phases mentioned in Section I. Each of these steps are carried out in different submodules, which will be explained hereafter.

A. Frontier Detection

First of all, candidate locations to be explored are recognized using frontier detector algorithms over the occupancy grid (i.e. points that lie between known and unknown regions). Similar to [47], two frontier detectors based on Rapidly-exploring Random Trees (RRT), acting on the local and global maps respectively, are used. Local and globally detected frontier points are fused together with those detected by the Canny edge detection algorithm. The points are then filtered in order to reduce the number of frontiers to evaluate. First, all points detected more than 5 s ago are discarded. Then, the remaining points are clustered using the Mean Shift algorithm (bandwidth of 1.5 m), storing the cluster centroids only. Finally, candidate frontiers are also discarded if: (i) they lie in occupied cells of the map, (ii) they are very close to the robot (Euclidean distance below 0.25 m), or (iii) the map information in the frontier's neighborhood is extremely low. This last filtering aims at deleting isolated unknown cells that could be wrongly detected as frontiers, and builds upon the fact that entropy can be efficiently approximated by the number of unknown cells in an occupancy map [48]. Therefore, if the percentage of unknown area within a 1 meter radius is less than 15%, the frontier is discarded (i.e. low expected information gain).

B. Decision Making

In order to select the most informative frontier, the following sequence is executed:

- i) compute the path to every frontier,
- ii) hallucinate a weighted pose-graph along every path,
- iii) compute $D\text{-}opt$ of every hallucinated graph, and
- iv) select the frontier with highest associated $D\text{-}opt$.

Thus, for every frontier, we firstly compute the path to reach it using only the global planner (Dijkstra's algorithm) of the `move_base` ROS package. Then, the existing pose-graph from the SLAM algorithm is expanded so as to contain

the effect of the predicted path. In order to do so, we add nodes randomly distributed along the predicted trajectory (the longer the path the greater number of nodes) and one final node at the frontier's location (see Figures 8a and 8b). Note that this procedure evaluates one single hypothesis per frontier. Future work will aim to study the effect of predicting multiple hypothesis of the posterior graph, but it has not been considered critical for the experiment's purpose. All these nodes are connected sequentially through odometry constraints. The j -th odometry constraint in the hallucinated pose-graph will have associated an Information matrix in the form:

$$\Phi_j = \Sigma_{\text{odom}}^{-1} * (1 + \chi) \quad (80)$$

where Σ_{odom} is the covariance matrix of the (Gaussian) transition noise:

$$\Sigma_{\text{odom}} = \begin{pmatrix} 0.04 & 0.001 & 0 \\ 0.001 & 0.04 & 0 \\ 0 & 0 & 0.008 \end{pmatrix} \quad (81)$$

Note that more distant frontiers will lead to larger uncertainties. The function of the parameter χ is to account for the effect of future measurements in the map. The map entropy reduction can be approximated as the number of unknown cells observable from the predicted node [49]. Thus, the normalized variable χ can be defined as:

$$\chi = \frac{C_U(\mathcal{M}_v)}{C(\mathcal{M}_v)} \quad (82)$$

with $\mathcal{M}_v \subset \mathcal{M}$ the sub-map in the node's vicinity (1.5 m radius), $C_U(\mathcal{M}_v)$ the number of unknown cells in that sub-map and $C(\mathcal{M}_v)$ the total amount of cells in it. This approach is similar to [19], but taking into account the whole pose-graph instead of just the *action pose-graph* (no initial factor needed), and also making Φ_j neither block-isotropic nor constant. It is dependent on the candidate actions, the future expected measurements and the map.

Also, if any of the predicted nodes is located near other existing nodes in the SLAM graph (Euclidean distance less than 2 m), we consider that a loop closure may occur. Let n_k denote the last known node, n_c a loop closure candidate (both from the SLAM graph) and n_p the predicted node in the hallucinated graph. We consider there is a loop closure probability between n_p and n_c if there is a minimum overlap of 15% between the area previously sensed from n_c and that expected to be sensed from n_p . This limitation avoids adding re-observation constraints, e.g., between oppositely oriented node pairs that fulfill the distance restriction. If it holds, a loop closure constraint is added with Information matrix:

$$\Phi_j = \mathbb{P}_{\text{LC}} * (\Delta\Phi_{n_k, n_c} * \psi) \quad (83)$$

where $\Delta\Phi_{n_k, n_c}$ is the information difference between the last known node and the candidate's, and ψ is the normalized number of nodes included inside the loop. Thus, this will encourage re-visiting areas with much higher (or lower) information. Also, re-observation between nearly consecutive edges will result in small weights and thus will have little effect in metrics of the weighted graph. Finally, \mathbb{P}_{LC} is the loop closing probability and can be computed as a function of the structure of

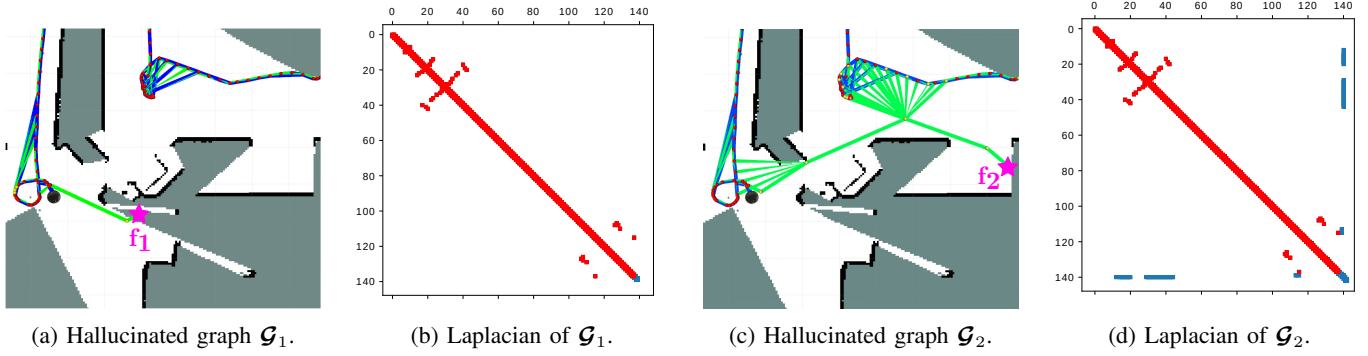


Fig. 8: Example of the graph hallucination to two different frontiers (magenta stars), and the sparsity patterns of the graph Laplacians. In images (a) and (c), nodes and edges of the SLAM pose-graph are shown in red and blue, while those of the hallucinated graph are depicted in yellow and green. Images (b) and (d) contain the sparsity patterns of the Laplacians of the SLAM graph (red) and the hallucinated pose-graph (blue). Note that red elements are overlapped and belong to both Laplacians.

the surrounding environment, that is, the number of occupied cells in the same vicinity χ was computed in. Embedding the loop closing probability directly in the FIM is possible since the graph weight fulfills $\gamma_j = \mathbb{P}_{LC} * \|\Phi_j\|_0 = \|\mathbb{P}_{LC} * \Phi_j\|_0$.

Figures 8c and 8d show an example of loop closure prediction, and the consequent effect in the Laplacian of the hallucinated graph. Depending on the size of the loop and the computed probability, each edge will encode different information.

Last step requires the computation of D -optimality criterion for all candidate locations. This criterion has been selected based on its capability of better capturing uncertainty, despite having shown higher approximation errors than T - and \tilde{E} -opt in the previous section. To do so, the weights of the pose-graph must be defined as $\gamma_j = \|\Phi_j\|_0$, and then, the weighted number of spanning trees has to be computed following (72). Note that weights encode the uncertainty of both the robot and the map representation. Then, the frontier with highest D -opt will be the optimal goal destination.

C. Action Execution

Finally, local planner of `move_base` deals with the execution of the planned path towards the selected frontier. Details of the configuration of this package can be found in the released code.

D. Simulation Results

As mentioned before, a ROS Noetic and Gazebo simulator framework has been used to test the approach. The robot is a wheeled platform equipped with a laser sensor with 180° field of view, 5m range and 1500 beams in each scan. The maximum linear and angular velocities of the robot are 0.2ms^{-1} and 0.8rads^{-1} , respectively. Additional configuration parameters can be found in the released code. The robot has been deployed on a slightly modified version of `willowgarage` office environment, which is about 2550m^2 ($\approx 56 \times 45\text{m}$). Experiments have been performed on an Intel Core i9-10900K CPU @ 3.70GHz and a NVidia GeForce RTX 3070 8GB GPU. CPU has dealt with most of the

computations (including, for example, Gazebo simulation and SLAM) and GPU has been used for simulation of the laser sensor, visualization purposes and the most expensive and repetitive computations, e.g, evaluation of neighborhood areas in the map during decision making.

The proposed experiment consists of autonomously exploring as much of the environment as possible in 30 min. In order to benchmark our method, we have used five more agents that represent some traditional and some state-of-the-art publicly available approaches. For a fair comparison, all agents share SLAM, frontier detection and navigation modules. Decision making, however, is based on different methods:

- a) **Random**: just for comparison purposes, since its results strongly depend on variability and the frontier detector.
- b) **Closest** frontier (based on path's Euclidean distance).
- c) **RRT** exploration: the simplest agent that reasons about the optimal frontier. It employs a cost-utility function with an approximate measure of the expected map entropy [47].
- d) **SHRE**: this method combines the expected uncertainties in the map and the robot pose posteriors in the Shannon-Rényi entropy. First, it computes the map's entropy and D -opt criterion from the FIM of the pose-graph. Then, the former is corrected using Rényi entropy with $\alpha = (1 + D\text{-opt})/D\text{-opt}$ [19].
- e) **Naive D-opt**: equivalent to the method described in Section V-B, but computing D -opt of the full FIM instead of using the graph topology.
- f) **Graph D-opt (ours)**.

Table II contains a quantitative comparison between all agents. Experiments have been repeated four times to get statistically consistent results, showing mean and, where appropriate, standard deviation. We present relevant metrics to compare their performance, both in terms of the map built and the pose-graph generated (i.e. trajectory) during exploration. On the one hand, this table shows results for the map size, area explored, coverage (percentage of explored area), max. Root Mean Squared Error (RMSE) found in the map, and number of graph optimizations performed due to loop closings. On the other hand, we provide several metrics of the graphs, namely:

Agent \ Metric		Random	Closest	RRT [47]	SHRE [19]	Naive D-opt	Ours
Map	Size (m)	36×33	45×28	36×25	35×20	26×28	30×30
	Area (m ²)	1143 ± 82	1245 ± 347	843 ± 65	695 ± 39	704 ± 60	840 ± 75
	Coverage (%)	23.5 ± 1.7	27.6 ± 2.6	22.3 ± 2.2	16.1 ± 0.8	14.4 ± 0.7	20.0 ± 1.7
	RMSE (m)	0.53 ± 0.17	1.41 ± 0.30	0.37 ± 0.07	0.22 ± 0.07	0.26 ± 0.05	0.30 ± 0.09
	Graph optim.	11	1	9	11	11	18
Graph	n	1477 ± 146	1346 ± 46	1307 ± 45	1044 ± 23	1067 ± 70	1527 ± 38
	\bar{d}	2.54 ± 0.13	2.77 ± 0.03	2.56 ± 0.05	2.40 ± 0.03	2.60 ± 0.05	2.54 ± 0.03
	$\log t_\gamma(\mathcal{G}) \cdot 10^{-4}$	1.16 ± 0.10	1.20 ± 0.09	1.03 ± 0.04	0.81 ± 0.02	0.85 ± 0.06	1.22 ± 0.02
	$\bar{\tau}(\mathcal{G}) \cdot 10^2$	5.57 ± 0.85	7.66 ± 0.31	6.05 ± 0.41	4.76 ± 0.34	6.59 ± 0.39	5.73 ± 0.19
	$\bar{\lambda}_2 \cdot 10^4$	0.74 ± 0.35	0.17 ± 0.06	0.61 ± 0.11	1.64 ± 0.57	1.34 ± 0.45	2.07 ± 0.88
Time	T _{DM} (%)	—	—	5.2 ± 0.7	33.7 ± 2.8	28.3 ± 1.5	3.2 ± 0.8

TABLE II: Comparison of different map and graph metrics after 30 minute exploration for the six agents. Results contain the mean and the standard deviation over four experiments. Best results among the four agents that reason are boldfaced.

the no. of nodes (n) and average node degree (\bar{d}), weighted tree connectivity, $\log t_\gamma(\mathcal{G})$, normalized tree connectivity [24], $\bar{\tau}(\mathcal{G}) \triangleq \log(t(\mathcal{G})) / ((n-2) \log(n))$, and normalized Fiedler value ($\bar{\lambda}_2$). Also, it contains the percentage of time dedicated to decision making. For every metric presented but for RMSE and time, higher is better.

As one could expect, the closest agent reports the best values for map size and coverage, at the expense of the highest RMSE. Exploiting the known environment is of no concern to this agent, which reflects in the absence of loop closures. The low normalized Fiedler value demonstrates the existence of isolated areas that make the graph nearly disconnected. RRT improves the previous results, creating a much more accurate map thanks to loop closures, and a slightly better connected graph. The heuristic rules this agent uses for decision making only required 5% of the total time. In contrast, SHRE map is very precise, at the cost of a significant computational burden, devoting 1/3 of the time to decision making. This entailed exploration of much smaller areas in the same time horizon: almost half that of any other agent. The constructed pose-graph is well connected, although smaller. SHRE results should be carefully considered, as maintaining better estimates (and connectivity) is easier on smaller maps. Results of the agent based of the naive computation of $D-opt$ are similar to those of SHRE. While the latter appears to mainly focus on improving the map, the former seeks a balance between the map and the pose-graph. The fact that both methods behaved similarly demonstrates that combining mapping and localization uncertainties directly in the FIM (see Section V-B) can perform just as well as doing so in utility [19].

Finally, our method illustrates that building a large quality map and a well-structured graph at the same time is possible. On average, it reports RMSE comparable to SHRE and naive $D-opt$, in a 33% larger map thanks to the extremely low amount of time dedicated to decision making. In fact, it is even faster than RRT, and there is a decrease of an order of magnitude with respect to previous agents based on FIM calculations, once again validating time results from Section IV-B. The pose-graph is very dense, with more nodes than any other method, and the connectivity indices are comparable to those

of SHRE and naive $D-opt$, in spite of the difference in map size (high connectivity indices are more difficult to maintain). Fiedler value and weighted tree connectivity are by far the highest. It can be observed that naive $D-opt$ and RRT have higher normalized tree connectivity, although this metric is less meaningful. For example, adding many low-informative edges between nearly consecutive nodes would result in higher $\bar{\tau}(\mathcal{G})$ than a single constraint with high information between disconnected areas in the graph, as will be seen below. All in all, our method achieved a balance between exploring the most of the environment and maintaining low uncertainty estimates, outperforming any other studied agent.

Figure 9 contains an example of the maps and pose-graphs generated during the experiment, plotted on top of a complete map of the environment for ease of comparison (first and third row); and a circular representation of the pose-graphs (second and fourth row). In the latter, edges have been colored according to their weight, after normalization across agents: darker colors correspond to lower values and thus information. Note these results represent just one of the most representative experiments performed by each agent, so they must be carefully considered, especially in the random agent in which there is a larger variability. Results clearly support the previous analysis. The closest agent generated a broad map, although error in the estimates and drift soon accumulated due to the lack of exploitation. This is also reflected in the absence of inner edges in subfigure 9e. RRT outperformed the previous agents, generating a better structured graph and a reasonable map. Still, certain regions are weakly connected and only a few re-observation edges connect distant nodes in the graph. Maps and graphs from SHRE and naive $D-opt$ are much more precise and dense, at the expense of a very reduced explored area. Consequently, most nodes and edges are clustered near the robot's starting position. Our approach strikes a balance between all the previous agents, standing out with respect to them. There is a consistent and large map at the same time that the graph is dense and well distributed. Subfigure 9l shows how edges are disseminated throughout the graph and connect distant nodes with high information. Circular plots show that higher \bar{d} and $\bar{\tau}(\mathcal{G})$ in other agents (e.g. RRT) reflect nearly

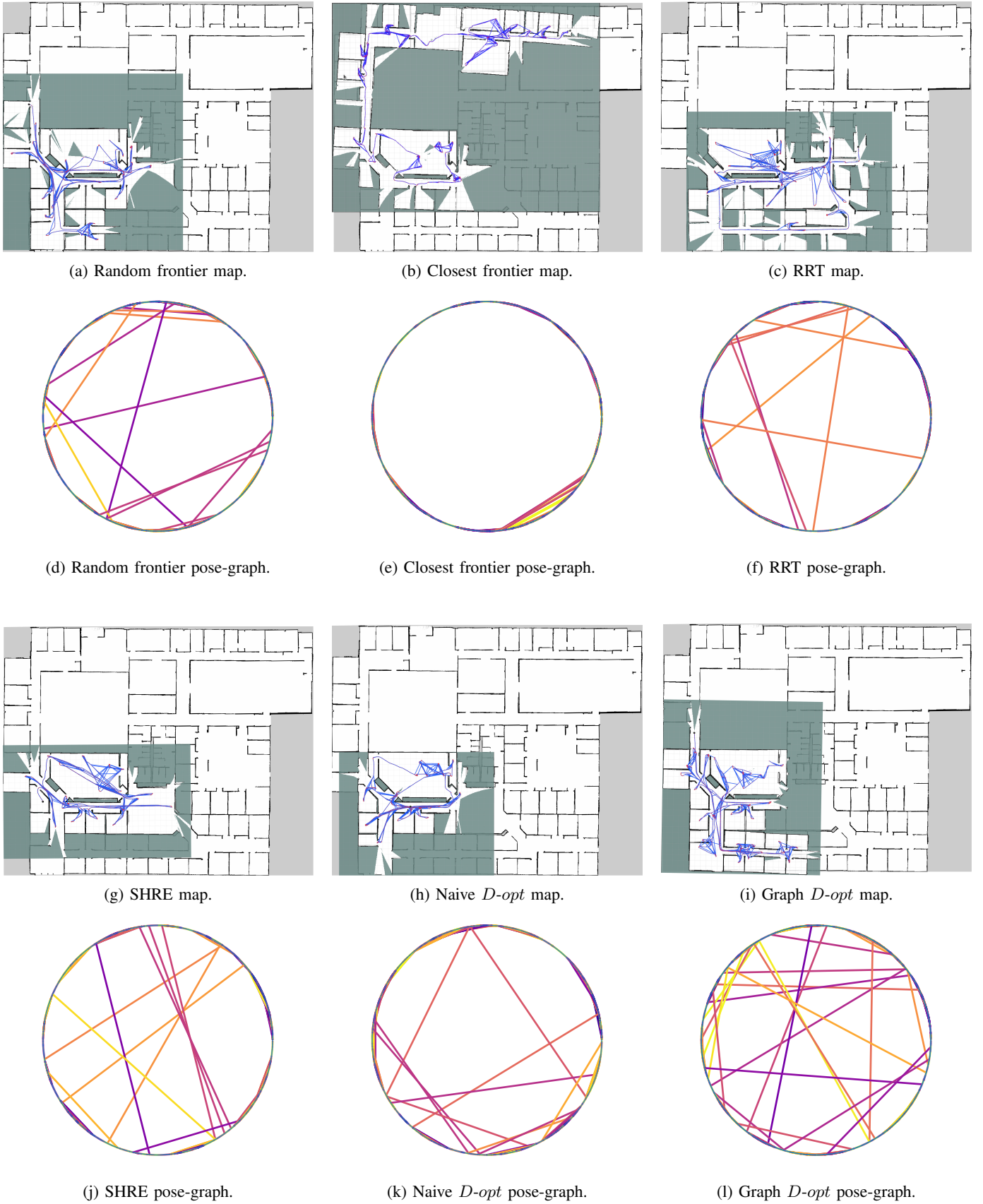


Fig. 9: Maps and pose-graphs generated by each agent after 30 minutes of autonomous exploration (first and third rows). The complete unknown map of the environment is depicted in the background for the ease of comparison. Also, circular representations of the respective pose-graphs (second and fourth rows). Edges are colored by weight, being darker lower.

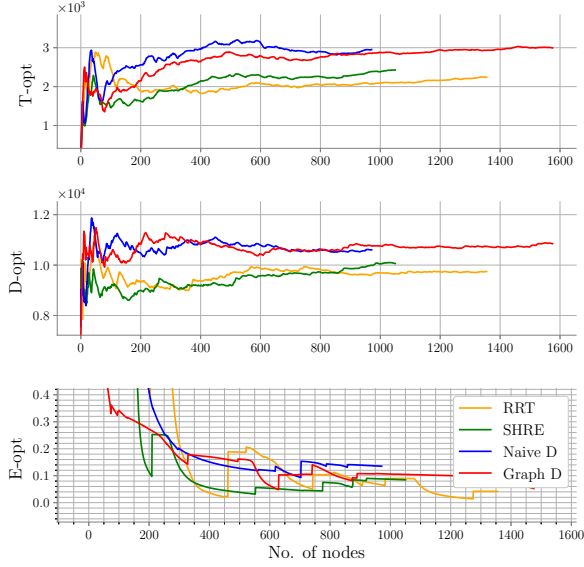


Fig. 10: Evolution of T -, D - and E -opt of the FIM during exploration with RRT (orange), SHRE (green), naive D -opt (blue) and our method (red).

consecutive and low-informative edges.

In order to compare naive and graph computation of D -opt, they have been simultaneously evaluated in the same experiment in Gazebo. Errors in the approximation of the graph D -opt ranged from 1 to 4%, and in all cases both methods led to the same decision. Mean error was 2.55%, a very similar value to those shown in Section IV-B.

Lastly, Figure 10 contains the evolution of T -, D - and E -opt (computed using the graph Laplacian) during the same experiments shown in Figure 9. Only the four intelligent agents are shown, namely RRT (orange), SHRE (green), naive D -opt (blue) and our method (red). Comparison between agents must be done carefully, since each of them explored different areas and generated different trajectories. T - and D -opt share the same clear trend. On the one hand, naive and graph D -opt performed very similar; as did SHRE and RRT. Also, RRT reached a permanent regime (especially in D -opt). On the other hand, naive and graph D -opt clearly outperformed SHRE and RRT. This is a key fact, since the former two rely on the method proposed in Section V-B to predict the pose-graph and its weights. Embedding the map information directly in the edge FIMs performed better than the heuristic rules of RRT and Shannon-Rényi entropy. Regarding E -opt (strongly linked to $\bar{\lambda}_2$), RRT shows the smallest values, reflecting the weak connectivity of some parts of the graph.

VI. CONCLUSIONS

In this paper, we have shown that quantifying uncertainty in active graph-SLAM formulated over the Lie group $SE(n)$ can be efficiently done by analyzing the topology of the underlying pose-graph. We have proposed and validated relationships between modern optimality criteria and graph connectivity

indices; showing that equivalent results can be obtained in a fraction of the time. On average, approximations with 2% error can be computed in 10% of the time. Moreover, the same trend is always maintained, demonstrating that that minimum uncertainty actions can be chosen by exploiting the graphical structure of the problem.

We leveraged this formulation to build an open-source on-line active SLAM method. It incorporates both robot and map uncertainties into the graph weights, and is capable of selecting D -optimal actions in significantly less time than other state-of-the-art methods based on expensive FIM computations. Online simulation experiments confirmed the previous results, estimating D -opt in 10% of the time traditional methods would require, with 2.55% error. Experiments also demonstrate that it clearly outperforms both traditional and heuristic fast exploration methods.

As future work, we aim to perform experiments with visual SLAM and a robotic platform in real world. Also, the use of full graphs instead of just pose-graphs is to be studied.

APPENDIX A

LIE GROUPS THEORY FUNDAMENTALS

A robot's pose and its uncertainty can be defined over Lie groups [37], [38] by using the special Euclidean group $SE(n')$ that represents rotations and translations, both for 2D and 3D spaces, as:

$$SE(n') \triangleq \left\{ \mathbf{g} = \begin{pmatrix} \mathbf{R} & \mathbf{p} \\ \mathbf{0} & 1 \end{pmatrix} \mid \mathbf{R} \in SO(n'), \mathbf{p} \in \mathbb{R}^{n'} \right\} \quad (84)$$

$\in \mathbb{R}^{(n'+1) \times (n'+1)}$

where $SO(n')$ is the special orthogonal group defined by:

$$SO(n') \triangleq \{ \mathbf{R} \in \mathbb{R}^{n' \times n'} \mid \mathbf{R}\mathbf{R}^T = \mathbf{I}, \det(\mathbf{R}) = 1 \} \quad (85)$$

Associated to every Lie group, there exists a tangent vector space (i.e. the space of differential transformations) around its identity element which fully captures its properties locally. It is known as the Lie algebra and is denoted as $\mathfrak{se}(n')$ and $\mathfrak{so}(n')$, for the special Euclidean and special orthogonal groups, respectively. The Lie algebras map spatial coordinates to spatial velocity. Elements of the Lie algebra $\mathfrak{se}(n')$ are represented as matrices contained in $\mathbb{R}^{(n'+1) \times (n'+1)}$, which are generated from tangent vectors contained in \mathbb{R}^ℓ , being ℓ the number of degrees of freedom of the space ($\ell = n'(n'+1)/2$). The hat operator of the special Euclidean group is defined as $\hat{\cdot} : \mathbb{R}^\ell \rightarrow \mathbf{H} \in \mathbb{R}^{(n'+1) \times (n'+1)}$, and it allows to generate elements of the Lie algebra $\mathfrak{se}(n')$ from tangent vectors. Let $\mathbf{d} = (\boldsymbol{\omega}, \mathbf{v})^T$ be such generic vector. Then,

$$\hat{\mathbf{d}} = \begin{pmatrix} [\boldsymbol{\omega}]_\times & \mathbf{v} \\ \mathbf{0} & 0 \end{pmatrix} \in \mathfrak{se}(n') \quad (86)$$

where $[\boldsymbol{\omega}]_\times$ is the skew symmetric matrix corresponding to the hat operator in $\mathfrak{so}(n')$. This operator is defined as $[\cdot]_\times : \mathbb{R} \rightarrow \mathbf{H} \in \mathbb{R}^{2 \times 2}$ and $[\cdot]_\times : \mathbb{R}^3 \rightarrow \mathbf{H} \in \mathbb{R}^{3 \times 3}$ for 2 and 3D, respectively. For the 2D case in which $\boldsymbol{\omega} = d\theta$ and $\mathbf{v} = (dx, dy)$, it will be:

$$[\boldsymbol{\omega}]_\times = \begin{pmatrix} 0 & -d\theta \\ d\theta & 0 \end{pmatrix} \in \mathfrak{so}(2) \quad (87)$$

And for the 3D case, where $\omega = (dw_x, dw_y, dw_z)$ and $v = (dx, dy, dz)$,

$$[\omega]_{\times} = \begin{pmatrix} 0 & -dw_z & dw_y \\ dw_z & 0 & -dw_x \\ -dw_y & dw_x & 0 \end{pmatrix} \in \mathfrak{so}(3) \quad (88)$$

The Lie algebra of the Euclidean group $SE(n')$ used in (86) may be formally defined as:

$$\mathfrak{se}(n') \triangleq \left\{ \hat{\xi} = \begin{pmatrix} [\omega]_{\times} & v \\ 0 & 0 \end{pmatrix} \mid [\omega]_{\times} \in \mathfrak{so}(n'), v \in \mathbb{R}^{n'} \right\} \quad (89)$$

$$\in \mathbb{R}^{(n'+1) \times (n'+1)}$$

with $\mathfrak{so}(n')$ the Lie algebra of $SO(n')$, which will be isomorphic to $\mathbb{R}^{n'}$ with the Lie bracket given by the cross product:

$$\mathfrak{so}(n') \triangleq [\omega]_{\times} \in \mathbb{R}^{n' \times n'} \mid \omega \in \mathbb{R}^{n'} \quad (90)$$

Elements of the Lie algebra and those of the underlying Lie group may be related through the exponential maps, which have a closed form. For the special Euclidean group, $\mathfrak{se}(n') \mapsto SE(n')$ is defined as:

$$\exp(\hat{\mathbf{d}}) = \left(\begin{array}{c|c} \exp([\omega]_{\times}) & \mathbf{V}v \\ \hline \mathbf{0} & 1 \end{array} \right) \quad (91)$$

where the exponential map $\exp([\omega]_{\times})$ is given for the 2D case as:

$$\exp([\omega]_{\times}) = \exp \begin{pmatrix} 0 & -d\theta \\ d\theta & 0 \end{pmatrix} = \begin{pmatrix} \cos(d\theta) & -\sin(d\theta) \\ \sin(d\theta) & \cos(d\theta) \end{pmatrix} \quad (92)$$

and,

$$\mathbf{V} = \begin{pmatrix} \frac{\sin(d\theta)}{\frac{d\theta}{1-\cos(d\theta)}} & -\frac{1-\cos(d\theta)}{\frac{d\theta}{\sin(d\theta)}} \\ \frac{1-\cos(d\theta)}{\frac{d\theta}{\sin(d\theta)}} & \frac{\sin(d\theta)}{\frac{d\theta}{1-\cos(d\theta)}} \end{pmatrix} \quad (93)$$

For the 3D case, $\exp([\omega]_{\times})$ is obtained as follows using the Rodrigues' formula:

$$\exp([\omega]_{\times}) = \mathbf{I} + \frac{\sin \theta}{\theta} [\omega]_{\times} + \frac{1 - \cos \theta}{\theta^2} [\omega]_{\times}^2 \quad (94)$$

where $\theta = \sqrt{\omega^T \omega}$, and,

$$\mathbf{V} = \begin{cases} \mathbf{I} & \text{if } \theta \rightarrow 0 \\ \mathbf{I} + \frac{1-\cos \theta}{\theta^2} [\omega]_{\times} + \frac{\theta - \sin \theta}{\theta^3} [\omega]_{\times}^2 & \text{otherwise} \end{cases} \quad (95)$$

APPENDIX B KRONECKER PRODUCT

Let \mathbf{A} be an $n \times m$ matrix and \mathbf{B} a $p \times q$ matrix. Then, their Kronecker product (denoted by \otimes) is a matrix \mathbf{C} of dimensions $(mp) \times (nq)$, which elements are given by:

$$c_{\alpha\beta} = a_{ij} b_{kl} \quad (96)$$

where $\alpha = p(i-1) + k$, and $\beta = q(j-1) + l$.

It can be expressed in matrix form as:

$$\mathbf{A} \otimes \mathbf{B} \triangleq \begin{pmatrix} a_{11}\mathbf{B} & \cdots & a_{1m}\mathbf{B} \\ \vdots & & \vdots \\ a_{1n}\mathbf{B} & \cdots & a_{mn}\mathbf{B} \end{pmatrix} \quad (97)$$

The Kronecker product satisfies the following properties:

- Associative and bilinear:

$$\mathbf{A} \otimes (\mathbf{B} + \mathbf{C}) = \mathbf{A} \otimes \mathbf{B} + \mathbf{A} \otimes \mathbf{C} \quad (98)$$

$$(\mathbf{B} + \mathbf{C}) \otimes \mathbf{A} = \mathbf{B} \otimes \mathbf{A} + \mathbf{C} \otimes \mathbf{A} \quad (99)$$

$$(k\mathbf{A}) \otimes \mathbf{B} = k(\mathbf{A} \otimes \mathbf{B}) = \mathbf{A} \otimes (k\mathbf{B}) \quad (100)$$

$$\mathbf{A} \otimes (\mathbf{B} \otimes \mathbf{C}) = (\mathbf{A} \otimes \mathbf{B}) \otimes \mathbf{C} \quad (101)$$

$$\mathbf{A} \otimes \mathbf{0} = \mathbf{0} \otimes \mathbf{A} = \mathbf{0} \quad (102)$$

- Non-commutative: $\mathbf{A} \otimes \mathbf{B} \neq \mathbf{B} \otimes \mathbf{A}$
- Mixed product: $(\mathbf{A} \otimes \mathbf{B})(\mathbf{C} \otimes \mathbf{D}) = (\mathbf{AC}) \otimes (\mathbf{BD})$
- Inverse (if \mathbf{A} and \mathbf{B} are invertible): $(\mathbf{A} \otimes \mathbf{B})^{-1} = \mathbf{A}^{-1} \otimes \mathbf{B}^{-1}$
- Transpose: $(\mathbf{A} \otimes \mathbf{B})^T = \mathbf{A}^T \otimes \mathbf{B}^T$

Consider now λ to be eigenvalue of \mathbf{A} with eigenvector \mathbf{x} and μ eigenvalue of \mathbf{B} with eigenvector \mathbf{y} , then $\lambda\mu$ will be eigenvalue of $\mathbf{A} \otimes \mathbf{B}$ with eigenvector $\mathbf{x} \otimes \mathbf{y}$. It can be proven using the eigenvalue equations:

$$\mathbf{A}\mathbf{x} = \lambda\mathbf{x} \quad \text{and} \quad \mathbf{B}\mathbf{y} = \mu\mathbf{y} \quad (103)$$

Then,

$$(\mathbf{A}\mathbf{x}) \otimes (\mathbf{B}\mathbf{y}) = (\lambda\mathbf{x}) \otimes (\mu\mathbf{y}) \quad (104)$$

And using the associative and mixed product properties:

$$(\mathbf{A} \otimes \mathbf{B})(\mathbf{x} \otimes \mathbf{y}) = \lambda\mu(\mathbf{x} \otimes \mathbf{y}) \quad (105)$$

Therefore, if $(\lambda_1, \dots, \lambda_n)$ and (μ_1, \dots, μ_p) are the sets of eigenvalues of \mathbf{A} and \mathbf{B} , then $(\lambda_i\mu_j : i = 1, 2, \dots, n \text{ and } j = 1, 2, \dots, p)$ is the set of eigenvalues of $\mathbf{A} \otimes \mathbf{B}$. In particular, the set of eigenvalues of $\mathbf{A} \otimes \mathbf{B}$ is the same as the one of $\mathbf{B} \otimes \mathbf{A}$. It follows that the trace and determinant of the Kronecker product are:

$$\text{trace}(\mathbf{A} \otimes \mathbf{B}) = \text{trace}(\mathbf{A})\text{trace}(\mathbf{B}) \quad (106)$$

$$\det(\mathbf{A} \otimes \mathbf{B}) = \det(\mathbf{A})^p \det(\mathbf{B})^n \quad (107)$$

APPENDIX C

RELATIONSHIP BETWEEN $\|\Sigma\|_p$ AND $\|Y\|_p$

Consider the graph covariance matrix Σ with eigenvalues $(\lambda_1, \dots, \lambda_\ell)$ and the graph information matrix \mathbf{Y} with eigenvalues $(\rho_1, \dots, \rho_\ell)$. Since $\mathbf{Y} = \Sigma^{-1}$,

$$\rho_k = \frac{1}{\lambda_k} \quad \forall k \quad (108)$$

Following (4), the p -norm of both matrices will be:

$$\|\Sigma\|_p = \begin{cases} \left(\frac{1}{\ell} \sum_{k=1}^{\ell} \lambda_k^p \right)^{\frac{1}{p}} & \text{if } 0 < |p| < \infty \\ \exp \left(\frac{1}{\ell} \sum_{k=1}^{\ell} \log(\lambda_k) \right) & \text{if } p \rightarrow 0 \end{cases} \quad (109)$$

and,

$$\|\Sigma^{-1}\|_p = \begin{cases} \left(\frac{1}{\ell} \sum_{k=1}^{\ell} \lambda_k^{-p} \right)^{\frac{1}{p}} & \text{if } 0 < |p| < \infty \\ \exp \left(\frac{1}{\ell} \sum_{k=1}^{\ell} \log \left(\frac{1}{\lambda_k} \right) \right) & \text{if } p \rightarrow 0 \end{cases} \quad (110)$$

The following general relationship may be established between them:

$$\|\Sigma^{-1}\|_p = (\|\Sigma\|_{-p})^{-1} \quad \forall p \quad (111)$$

Proof: For the case that $p \rightarrow 0$,

$$\|\Sigma^{-1}\|_0 = \exp\left(\frac{1}{\ell} \sum_{k=1}^{\ell} \log\left(\frac{1}{\lambda_k}\right)\right) \quad (112)$$

$$= \exp\left(\frac{1}{\ell} \sum_{k=1}^{\ell} -\log(\lambda_k)\right) \quad (113)$$

$$\therefore \|\Sigma^{-1}\|_p = (\|\Sigma\|_p)^{-1} \quad \text{if } p \rightarrow 0 \quad (114)$$

For $p = \pm 1$:

$$\|\Sigma^{-1}\|_1 = \frac{1}{\ell} \sum_{k=1}^{\ell} \lambda_k^{-1} \quad (115)$$

$$\|\Sigma^{-1}\|_{-1} = \left(\frac{1}{\ell} \sum_{k=1}^{\ell} \lambda_k\right)^{-1} \quad (116)$$

$$\|\Sigma\|_1 = \frac{1}{\ell} \sum_{k=1}^{\ell} \lambda_k \quad (117)$$

$$\|\Sigma\|_{-1} = \left(\frac{1}{\ell} \sum_{k=1}^{\ell} \lambda_k^{-1}\right)^{-1} \quad (118)$$

$$\therefore \|\Sigma^{-1}\|_p = (\|\Sigma\|_{-p})^{-1} \quad \text{if } p = \pm 1 \quad (119)$$

Finally, for $p \rightarrow \pm\infty$:

$$\|\Sigma^{-1}\|_{\infty} = \max(\rho_k) = \max(\lambda_k^{-1}) = \min(\lambda_k)^{-1} \quad (120)$$

$$\|\Sigma^{-1}\|_{-\infty} = \min(\rho_k) = \min(\lambda_k^{-1}) = \max(\lambda_k)^{-1} \quad (121)$$

$$\|\Sigma\|_{\infty} = \max(\lambda_k) \quad (122)$$

$$\|\Sigma\|_{-\infty} = \min(\lambda_k) \quad (123)$$

$$\therefore \|\Sigma^{-1}\|_p = (\|\Sigma\|_{-p})^{-1} \quad \text{if } p \rightarrow \pm\infty \quad (124)$$

APPENDIX D

EXTENDED VALIDATION RESULTS

This Appendix presents extended results for validation of Section III. Figure D.1 contains the results for \tilde{E} -, T -, D - and A -opt criteria of Σ computed with both methods; during the exploratory trajectory in FRH dataset (constant uncertainty case). Blue curves correspond to applying optimality criteria to the covariance matrix, while red ones do to applying them to L and $\tilde{\Sigma}$ matrices. Figure D.2 depicts optimality criteria computed with both methods, for MIT and INTEL datasets (variable uncertainty case), weighting the pose-graphs with the same criterion to be evaluated.

Finally, this Appendix contains results for the 3D Parking Garage dataset. The original dataset contains 1661 nodes and 6275 constraints, however, the amount of loop closure

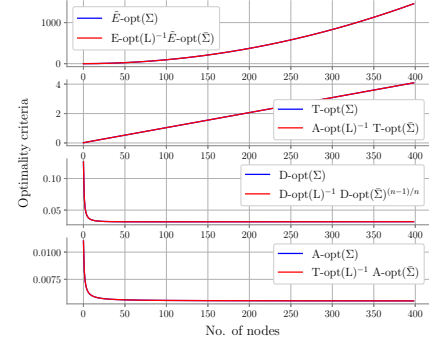
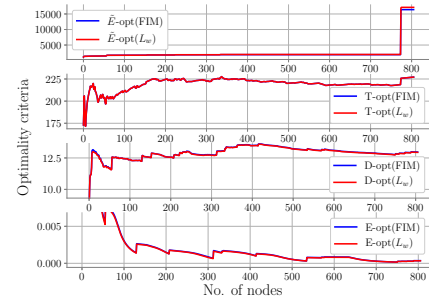
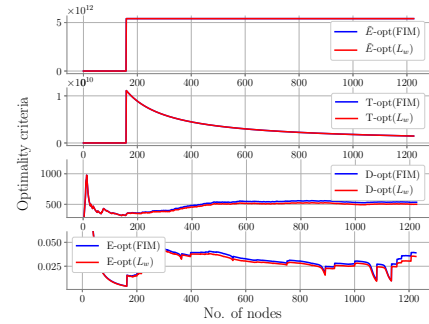


Fig. D.1: Optimality criteria of the covariance matrix (blue) and the Laplacian (red), for the reduced FRH dataset.



(a) MIT.



(b) INTEL.

Fig. D.2: Optimality criteria of the information matrix (blue) and the Laplacian (red) weighted with $\|\Phi_j\|_p$, for (a) MIT dataset and (b) INTEL.

edges has been arbitrarily reduced, making \mathbf{Y} more sparse and simplifying the computational complexity. Its trajectory is depicted in Figure D.3. The sparsity pattern of \mathbf{Y} appears in Figure D.4, showing the existence of numerous loop closures. The comparison between computing $\|\mathbf{L}_\gamma\|_p$ and $\|\mathbf{Y}\|_p$ in appears in Figure D.5. They are approximately equal during the entire trajectory despite evaluating a 3D pose-graph. Figure D.6 shows the time consumption of both methods. Behavior is equivalent to the one seen in Fig. 5, although now time is represented in a logarithmic scale; and there is a difference of more than 10^2 seconds between them in the end of the sequence.



Fig. D.3: Trajectory of the modified Garage 3D dataset, in which loop closures constraints also appear.

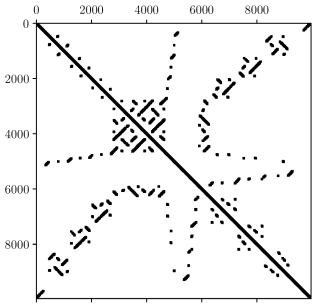


Fig. D.4: Sparsity pattern of the full FIM in the modified Garage dataset.

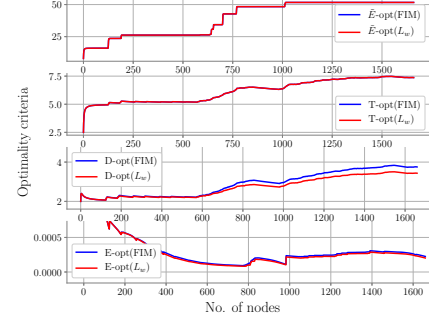


Fig. D.5: Optimality criteria of the information matrix (blue) and the Laplacian (red), weighted with $\|\Phi_j\|_p$, for Garage 3D dataset.

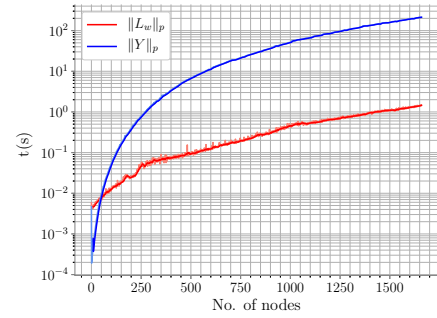


Fig. D.6: Log-linear plot of the time consumed (in sec.) at each step to compute optimality criteria of both approaches; for Garage 3D dataset.

REFERENCES

- [1] M. Montemerlo and S. Thrun, "Simultaneous localization and mapping with unknown data association using fastslam," in *2003 IEEE International Conference on Robotics and Automation (Cat. No. 03CH37422)*, vol. 2. IEEE, 2003, pp. 1985–1991.
- [2] G. Grisetti, R. Kummerle, C. Stachniss, and W. Burgard, "A tutorial on graph-based slam," *IEEE Intelligent Transportation Systems Magazine*, vol. 2, no. 4, pp. 31–43, 2010.
- [3] S. Thrun, W. Burgard, and D. Fox, *Probabilistic Robotics (Intelligent Robotics and Autonomous Agents)*. MIT Press, 2005.
- [4] H. Durrant-Whyte and T. Bailey, "Simultaneous localization and mapping: part i," *IEEE Robotics & Automation Magazine*, vol. 13, no. 2, pp. 99–110, 2006.
- [5] C. Cadena, L. Carlone, H. Carrillo, Y. Latif, D. Scaramuzza, J. Neira, I. Reid, and J. J. Leonard, "Past, present, and future of simultaneous localization and mapping: Toward the robust-perception age," *IEEE Transactions on Robotics*, vol. 32, no. 6, pp. 1309–1332, 2016.
- [6] W. Burgard, D. Fox, and S. Thrun, "Active mobile robot localization," in *1997 International Joint Conferences on Artificial Intelligence*, Nagoya, Japan, 1997, pp. 1346–1352.
- [7] H. J. S. Feder, J. J. Leonard, and C. M. Smith, "Adaptive mobile robot navigation and mapping," *The International Journal of Robotics Research*, vol. 18, no. 7, pp. 650–668, 1999.
- [8] H. Carrillo, I. Reid, and J. A. Castellanos, "On the comparison of uncertainty criteria for active slam," in *2012 IEEE International Conference on Robotics and Automation (ICRA)*. IEEE, Minnesota, USA, 2012, pp. 2080–2087.
- [9] B. Bonet and H. Geffner, "Planning with incomplete information as heuristic search in belief space," in *Proceedings of the Fifth International Conference on Artificial Intelligence Planning Systems*, 2000, pp. 52–61.
- [10] R. Platt Jr, R. Tedrake, L. Kaelbling, and T. Lozano-Perez, "Belief space planning assuming maximum likelihood observations," in *Proceedings of the Robotics: Science and Systems Conference*, 2010.
- [11] A. A. Makarenko, S. B. Williams, F. Bourgault, and H. F. Durrant-Whyte, "An experiment in integrated exploration," in *2002 IEEE/RSJ International Conference on Intelligent Robots and Systems (IROS)*, vol. 1. IEEE, Lausanne, Switzerland, 2002, pp. 534–539.
- [12] F. Pukelsheim, *Optimal design of experiments*. SIAM, 2006.
- [13] C. Stachniss, G. Grisetti, and W. Burgard, "Information gain-based exploration using rao-blackwellized particle filters," in *Robotics: Science and Systems*, vol. 2, 2005, pp. 65–72.
- [14] C. Leung, S. Huang, and G. Dissanayake, "Active slam using model predictive control and attractor based exploration," in *2006 IEEE/RSJ International Conference on Intelligent Robots and Systems*. IEEE, 2006, pp. 5026–5031.
- [15] L. Carlone, J. Du, M. K. Ng, B. Bona, and M. Indri, "Active slam and exploration with particle filters using kullback-leibler divergence," *Journal of Intelligent & Robotic Systems*, vol. 75, no. 2, pp. 291–311, 2014.
- [16] S. Bai, J. Wang, F. Chen, and B. Englot, "Information-theoretic exploration with bayesian optimization," in *2016 IEEE/RSJ International Conference on Intelligent Robots and Systems (IROS)*. IEEE, 2016, pp. 1816–1822.
- [17] Y. Chen, S. Huang, and R. Fitch, "Active slam for mobile robots with area coverage and obstacle avoidance," *IEEE/ASME Transactions on Mechatronics*, 2020.
- [18] R. Valencia Carreño, J. Valls Miró, G. Dissanayake, and J. Andrade-Cetto, "Active pose slam," in *Proceedings of the 2012 IEEE/RSJ International Conference on Intelligent Robots and Systems*, 2012, pp. 1885–1891.
- [19] H. Carrillo, P. Dames, V. Kumar, and J. A. Castellanos, "Autonomous robotic exploration using a utility function based on rényi's general theory of entropy," *Autonomous Robots*, vol. 42, no. 2, pp. 235–256, 2018.
- [20] V. Indelman, L. Carlone, and F. Dellaert, "Planning in the continuous domain: A generalized belief space approach for autonomous navigation in unknown environments," *The International Journal of Robotics Research*, vol. 34, no. 7, pp. 849–882, 2015.

- [21] K. Elimelech and V. Indelman, "Simplified decision making in the belief space using belief sparsification," *arXiv preprint arXiv:1909.00885*, 2019.
- [22] K. Khosoussi, S. Huang, and G. Dissanayake, "Novel insights into the impact of graph structure on slam," in *2014 IEEE/RSJ International Conference on Intelligent Robots and Systems*. IEEE, 2014, pp. 2707–2714.
- [23] C.-S. Cheng, "Maximizing the total number of spanning trees in a graph: two related problems in graph theory and optimum design theory," *Journal of Combinatorial Theory, Series B*, vol. 31, no. 2, pp. 240–248, 1981.
- [24] K. Khosoussi, M. Giamou, G. S. Sukhatme, S. Huang, G. Dissanayake, and J. P. How, "Reliable graphs for slam," *The International Journal of Robotics Research*, vol. 38, no. 2-3, pp. 260–298, 2019.
- [25] Y. Chen, S. Huang, L. Zhao, and G. Dissanayake, "Cramér-rao bounds and optimal design metrics for pose-graph slam," *IEEE Transactions on Robotics*, vol. 37, no. 2, pp. 627–641, 2021.
- [26] A. Kitanov and V. Indelman, "Topological information-theoretic belief space planning with optimality guarantees," *arXiv preprint arXiv:1903.00927*, 2019.
- [27] M. L. Rodríguez-Arévalo, J. Neira, and J. A. Castellanos, "On the importance of uncertainty representation in active slam," *IEEE Transactions on Robotics*, vol. 34, no. 3, pp. 829–834, 2018.
- [28] L. Mihaylova, T. Lefebvre, H. Bruyninckx, K. Gadeyne, and J. De Schutter, "A comparison of decision making criteria and optimization methods for active robotic sensing," in *International Conference on Numerical Methods and Applications*. Springer, 2002, pp. 316–324.
- [29] J. A. Placed and J. A. Castellanos, "Fast autonomous robotic exploration using the underlying graph structure," in *2021 IEEE/RSJ International Conference on Intelligent Robots and Systems (IROS)*. IEEE, 2021, pp. 6649–6656.
- [30] J. Kiefer, "General equivalence theory for optimum designs (approximate theory)," *The annals of Statistics*, pp. 849–879, 1974.
- [31] B. Zhou, "On sum of powers of the laplacian eigenvalues of graphs," *Linear Algebra and its Applications*, vol. 429, no. 8-9, pp. 2239–2246, 2008.
- [32] E. Fritscher, C. Hoppen, I. Rocha, and V. Trevisan, "On the sum of the laplacian eigenvalues of a tree," *Linear Algebra Appl.*, vol. 435, no. 2, pp. 371–399, 2011.
- [33] H. A. Ganie, S. Pirzada, R. Ul Shaban, and X. Li, "Upper bounds for the sum of laplacian eigenvalues of a graph and brouwer's conjecture," *Discrete Mathematics, Algorithms and Applications*, vol. 11, no. 02, p. 1950028, 2019.
- [34] N. M. M. De Abreu, "Old and new results on algebraic connectivity of graphs," *Linear algebra and its applications*, vol. 423, no. 1, pp. 53–73, 2007.
- [35] H. Chen and F. Zhang, "Resistance distance and the normalized laplacian spectrum," *Discrete Applied Mathematics*, vol. 155, no. 5, pp. 654–661, 2007.
- [36] M. Yadav, "Resistance distance, kirchhoff index, foster's theorems, and generalizations," Ph.D. dissertation, University of Oklahoma, 2017.
- [37] T. D. Barfoot and P. T. Furgale, "Associating uncertainty with three-dimensional poses for use in estimation problems," *IEEE Transactions on Robotics*, vol. 30, no. 3, pp. 679–693, 2014.
- [38] M. Brossard, S. Bonnabel, and J.-P. Condomines, "Unscented kalman filtering on lie groups," in *2017 IEEE/RSJ International Conference on Intelligent Robots and Systems (IROS)*. IEEE, 2017, pp. 2485–2491.
- [39] I. Gohberg and M. G. Kreĭn, *Introduction to the Theory of Linear Nonselfadjoint Operators*. American Mathematical Soc., 1978, vol. 18.
- [40] A. Wald, "On the efficient design of statistical investigations," *The annals of mathematical statistics*, vol. 14, no. 2, pp. 134–140, 1943.
- [41] L. Carlone, R. Aragues, J. A. Castellanos, and B. Bona, "A fast and accurate approximation for planar pose graph optimization," *The International Journal of Robotics Research*, vol. 33, no. 7, pp. 965–987, 2014.
- [42] L. Carlone, R. Tron, K. Daniilidis, and F. Dellaert, "Initialization techniques for 3d slam: a survey on rotation estimation and its use in pose graph optimization," in *2015 IEEE international conference on robotics and automation (ICRA)*. IEEE, 2015, pp. 4597–4604.
- [43] M. Burri, J. Nikolic, P. Gohl, T. Schneider, J. Rehder, S. Omari, M. W. Achtelik, and R. Siegwart, "The euroc micro aerial vehicle datasets," *The International Journal of Robotics Research*, vol. 35, no. 10, pp. 1157–1163, 2016.
- [44] C. Campos, R. Elvira, J. J. G. Rodríguez, J. M. Montiel, and J. D. Tardós, "Orb-slam3: An accurate open-source library for visual-inertial, and multimap slam," *IEEE Transactions on Robotics*, 2021.
- [45] K. Konolige, G. Grisetti, R. Kümmerle, W. Burgard, B. Limketkai, and R. Vincent, "Efficient sparse pose adjustment for 2d mapping," in *2010 IEEE/RSJ International Conference on Intelligent Robots and Systems*. IEEE, 2010, pp. 22–29.
- [46] G. Grisetti, R. Kümmerle, H. Strasdat, and K. Konolige, "g2o: A general framework for (hyper) graph optimization," in *Proceedings of the IEEE International Conference on Robotics and Automation (ICRA)*, Shanghai, China, 2011, pp. 9–13.
- [47] H. Umari and S. Mukhopadhyay, "Autonomous robotic exploration based on multiple rapidly-exploring randomized trees," in *2017 IEEE/RSJ International Conference on Intelligent Robots and Systems (IROS)*. IEEE, 2017, pp. 1396–1402.
- [48] C. Stachniss, *Robotic mapping and exploration*. Springer, 2009, vol. 55.
- [49] N. Palomeras, M. Carreras, and J. Andrade-Cetto, "Active slam for autonomous underwater exploration," *Remote Sensing*, vol. 11, no. 23, p. 2827, 2019.